GENETICS

Loss-of-function mutations in *CEP78* cause male infertility in humans and mice

Xueguang Zhang[1]†, Rui Zheng[1]†, Chen Liang[2]†, Haotian Liu[3]†, Xiaozhen Zhang[4]†, Yongyi Ma[5], Mohan Liu[1], Wei Zhang[6], Yang Yang[7], Man Liu[1], Chuan Jiang[1], Qingjia Ren[2], Yan Wang[8]*, Suren Chen[4]*, Yihong Yang[8]*, Ying Shen[1]*

Centrosomal protein dysfunction might cause ciliopathies. However, the role of centrosomal proteins in male infertility remains poorly defined. Here, we identified a pathogenic splicing mutation in *CEP78* in male infertile patients with severely reduced sperm number and motility, and the typical multiple morphological abnormalities of the sperm flagella phenotype. We further created *Cep78* knockout mice, which showed an extremely low sperm count, completely aberrant sperm morphology, and approximately null sperm motility. The infertility of the patients and knockout mice could not be rescued by an intracytoplasmic sperm injection treatment. Mechanistically, CEP78 might regulate USP16 expression, which further stabilizes Tektin levels via the ubiquitination pathway. *Cep78* knockout mice also exhibited impairments in retina and outer hair cells of the cochlea. Collectively, our findings identified nonfunctional CEP78 as an indispensable factor contributing to male infertility and revealed a role for this gene in regulating retinal and outer hair cell function in mice.

INTRODUCTION

The World Health Organization (WHO) has deemed infertility to be a global health problem, and the negative impact of infertility has affected both developed and developing countries (*1*). Male infertility, which affects approximately 20 to 70% of couples facing infertility (*2*), is mainly attributed to a decreased sperm count (azoospermia or oligozoospermia), attenuated sperm motility (asthenozoospermia), or a greater proportion of morphologically abnormal sperm (teratozoospermia). Factors leading to male infertility include urogenital infections, immune or hormone abnormalities, and genetic diseases (*3*). Although male infertility is multifactorial, it has a strong genetic basis that still has not been completely clarified.

The centrosome is a subcellular organelle composed of two centrioles embedded in pericentriolar material that is present in most eukaryotic cells and plays a critical role in various cellular processes, including cell division, motility, and cilia formation (*4*). The centrosome is essential for reproductive biology. First, during spermatogenesis, the centrosome is required to form the integral spermatozoon structure, including the sperm flagellum and head-tail coupling apparatus. Second, in fertilization, the centrosome forms the major microtubule-organizing center that contributes to the movement and fusion of the male and female pronuclei; after completing replication and splitting, the sperm centrosome organizes the bipolar array that forms the mitotic spindle required for cleavage (*5*). The molecular composition of the centrosome is complex, consisting of hundreds of proteins known as centrosomal proteins. Therefore, defects in the functions of centrosomal proteins are presumed to be linked to male infertility, but the relevant findings are limited. Loss-of-function variants in centrosomal protein of 135 kDa (*CEP135*) and *CEP112* account for multiple morphological abnormalities of the sperm flagella (MMAF) and acephalic spermatozoa phenotypes, respectively, in humans (*6*, *7*), and *Cep55*, spermatogenesis associated 6 (*Spata6*), *Cep131*, *Cep164*, centrin 1 (*Cetn1*), and spermatogenesis and centriole associated 1 like (*Spatc1l*) are suggested to be involved in mouse infertility (*8*–*13*). To date, only the centrosomal proteins of testis specific 10 (TSGA10) and CEP128 have been shown to be associated with male sterility in both humans and mice (*14*–*16*).

CEP78 is a centriole wall protein that localizes to mature centrioles and is involved in regulating centrosome duplication (*17*). CEP78 is generally expressed in ciliated organisms, suggesting that CEP78 might be involved in cilia biogenesis and/or function in several organisms (*18*). Biallelic inactivating variants in *CEP78* have been linked to autosomal recessive cone-rod dystrophy with hearing loss (CRDHL) syndrome [OMIM (Mendelian Inheritance in Man) no. 617236] in humans (*19*–*22*). However, the biological function of CEP78 in male reproduction remains poorly characterized.

In the present study, we identified the previously unreported homozygous splicing mutation c.1069+1G>A in *CEP78* in an infertile family through whole-exome sequencing (WES). The patients presented a characteristic MMAF phenotype, including coiled, bent, irregular, short, or/and absent flagella and defects in sperm flagellar ultrastructure. We further generated *Cep78* knockout (KO) mice, and the phenotype of *Cep78* KO male mice resembled the infertile phenotype of the patients, showing marked defects in sperm count, morphology, and motility. Functionally, we showed that CEP78 promotes the expression of the deubiquitinating enzyme ubiquitin specific peptidase 16 (USP16), which stabilizes Tektin expression via the ubiquitination pathway. In addition to the infertile phenotype,

[1]Department of Obstetrics/Gynecology, Key Laboratory of Obstetric, Gynecologic and Pediatric Diseases and Birth Defects of Ministry of Education, West China Second University Hospital, Sichuan University, Chengdu 610041, China. [2]Department of Ophthalmology, West China Hospital of Sichuan University, Chengdu 610041, China. [3]Department of Otolaryngology–Head and Neck Surgery, West China Hospital of Sichuan University, Chengdu 610041, China. [4]Key Laboratory of Cell Proliferation and Regulation Biology, Ministry of Education, Department of Biology, College of Life Sciences, Beijing Normal University, Beijing 100875, China. [5]Department of Gynecology and Obstetrics, Southwest Hospital, Third Military Medical University (Army Medical University), Chongqing 400000, China. [6]Mental Health Center and Psychiatric Laboratory, State Key Laboratory of Biotherapy, West China Hospital of Sichuan University, Chengdu 610041, China. [7]State Key Laboratory of Biotherapy and Cancer Center, West China Hospital, Sichuan University and Collaborative Innovation Center, Chengdu 610041, China. [8]Reproduction Medical Center of West China Second University Hospital, Key Laboratory of Obstetric, Gynecologic and Pediatric Diseases and Birth Defects of Ministry of Education, Sichuan University, Chengdu 610041, China.
*Corresponding author. Email: wangyy1210@163.com (Y.W.); chensr@bnu.edu.cn (S.C.); yyhpumc@foxmail.com (Y.Y.); yingcaishen01@163.com (Y.S.)
†These authors contributed equally to this work.

we observed deficient function of the retina and outer hair cells of the cochlea (OHCs) in *Cep78* KO mice, as *CEP78* mutations have been suggested to cause CRDHL syndrome in humans. Together, we elucidated *CEP78* as a causative gene of male infertility in both humans and mice, providing unexplored insights into the roles of centrosomal proteins in reproductive biology.

RESULTS

Identification of a *CEP78* splicing mutation in a large family with male infertility

A 28-year-old man from a consanguineous family who was diagnosed with 7 years of primary infertility was recruited for our study. The somatic cell karyotype (46, XY), bilateral testicular size, secondary sex characteristics, and hormone levels were normal. A semen analysis of this patient revealed an extremely reduced sperm count and motility as well as an abnormal sperm morphology (table S1). In addition to the proband, two other male individuals in this family were affected, his brother (IV-8) and great uncle (II-5), who had never conceived during their marriages or while engaging in unprotected sexual intercourse. Noticeably, the patient indicated that he also suffered from hearing and vision defects, and his great uncle (II-5) and great aunt (II-4, deceased) had experienced similar problems. We further performed vision and hearing tests on the proband, and color fundus photography (CFP) revealed some tessellated fundus changes, indicating thinning of the retina (Fig. 1A). Using optical coherence tomography (OCT), we also found that the outer nuclear layer (ONL) was thinning and that the inner segment/outer segment (IS/OS) layer was becoming blurred (Fig. 1B). The otoscopic examination showed that the tympanic membranes in both ears of the patient were intact (Fig. 1C), and the acoustic immittance test results were also normal (Fig. 1D). However, acoustic reflection was not detected in the bilateral ears (Fig. 1E), suggesting that obstacles to the auditory conduction pathway may be present. In addition, the binaural pure-tone hearing threshold test of the patient showed that the 1.5- to 8-kHz threshold was 40 to 80 decibel hearing level (dB HL) (normal range, ≤20 dB HL) (Fig. 1F), indicating that the proband had bilateral sensorineural hearing loss associated with moderate-to-severe defects in the mid-to-high frequency hearing threshold.

Aiming to illuminate the genetic cause of the phenotype in this family, we performed WES analysis on the proband. Consequently, the previously unidentified homozygous splicing mutation c.1069+1G>A in *CEP78* was suggested to be the potential genetic cause of oligoasthenoteratospermia and hearing and vision defects afflicting this patient (fig. S1, A and B). This variant was absent in any of the population databases. Moreover, this variant was predicted to be most probably affecting splicing according to the Human Splicing Finder tool (*23*) and was predicted to be disease causing by MutationTaster tool (*24*). Sanger sequencing was performed on this large family, and his unaffected parents (III-7 and III-8), sister (IV-7), and aunt (III-6) harbored a heterozygous variant of c.1069+1G>A; as expected, his infertile brother (IV-8) and great uncle (II-5) were carriers of this identical homozygous variant (Fig. 1G). In addition, Sanger sequencing verification of 1000 normal controls did not reveal this variant.

We initially used real-time polymerase chain reaction (RT-PCR) using RNA from blood leukocytes of the proband and the normal control to amplify a fragment of *CEP78* mRNA and study the effect of the c.1069+1G>A mutation in *CEP78* on splicing. The electrophoresis results showed a measurable increase in the molecular weight of the mutant fragment [632 base pairs (bp)] compared to the normal control fragment (514 bp) (Fig. 1H). Sanger sequencing further revealed that the variant caused the retention of 121 nucleotides of intron 8 in exon 8 and three nucleotide deletions in the 5′ end of exon 9 in *CEP78* (Fig. 1H), which was expected to translate a truncated protein due to a frameshift and premature termination codon (p.Gly357Aspfs*13) (fig. S1C). A functional splicing reporter minigene assay validated this negative effect of the mutation on *CEP78* splicing in vitro (fig. S1, D to F). We further constructed a mutant plasmid containing the abnormal complementary DNA (cDNA) sequence of *CEP78* caused by the splicing mutation, and the Western blotting results revealed no CEP78 expression in cells transfected with mutant *CEP78* plasmid compared to the wild-type (WT)–*CEP78* plasmid (Fig. 1I). Therefore, this *CEP78* splicing mutation leading to a lack of protein expression is suggested to be the genetic cause of male infertility and hearing and visual impairment in this family.

Confirmation of the oligoasthenoteratospermia phenotype in the two siblings

CEP78 is a known causative gene for CRDHL syndrome, which is characterized by cone-rod dystrophy and sensorineural hearing loss, with relatively late onset of both ocular and auditory impairments (*19*–*22*). Thus, our proband showed defects in hearing and vision. However, the association of infertility with *CEP78* mutations is largely unknown. We subsequently collected semen samples from the two siblings to explore the spermatozoa phenotypic characteristics associated with *CEP78* mutation. An evaluation of sperm morphology of the two siblings using Papanicolaou staining and scanning electron microscopy (SEM) revealed various malformations in sperm morphology, including short, absent, coiled, bent, and irregular flagella as well as anomalous heads (Fig. 2, A and B, and fig. S2A). Transmission electron microscopy (TEM) was used to analyze the ultrastructure of spermatozoa from the two siblings. Numerous sperm nuclei were deformed, including small, tapering, or pyriform shapes, and the chromatin was more condensed or rarefactional than that of the control (Fig. 2C and fig. S2B). In the sperm-connecting piece, the proximal centriole (PC) was defective, showing the disordered, incomplete, or totally absent triplet microtubule, and some splayed microtubules of distal centriole were shorter or were completely missing, while the segmented column (Sc) and basal plate (Bp) were present (Fig. 2D and figs. S2C and S3). Notably, an irregular "9 + 2" structure of the sperm flagella was observed in the midpiece, where the peripheral microtubule doublets (MTDs) and outer dense fibers (ODFs) were disordered and missing, and the central pairs (CPs) were constantly absent; a lack of the CPs and MTDs, accompanied by shambolic arrangements of ODFs, was observed in the principal piece of most flagella; in addition, the axoneme was frequently missing in the end piece (Fig. 2E and figs. S2D and S3). Some unorganized axoneme clusters from several flagellar pieces were wrapped by a single piece in the sperm of the two patients (Fig. 2F). Together, these observations suggested that the loss-of-function mutations of *CEP78* are also associated with oligoasthenoteratospermia and subsequently cause male infertility.

Characterization of the infertile phenotype of homozygous *Cep78* KO male mice

The mammalian sperm centrosome is remodeled during spermiogenesis, and centrosomal proteins are eliminated, reduced, enriched, or redistributed (*25*). CEP78 was undetectable in human mature

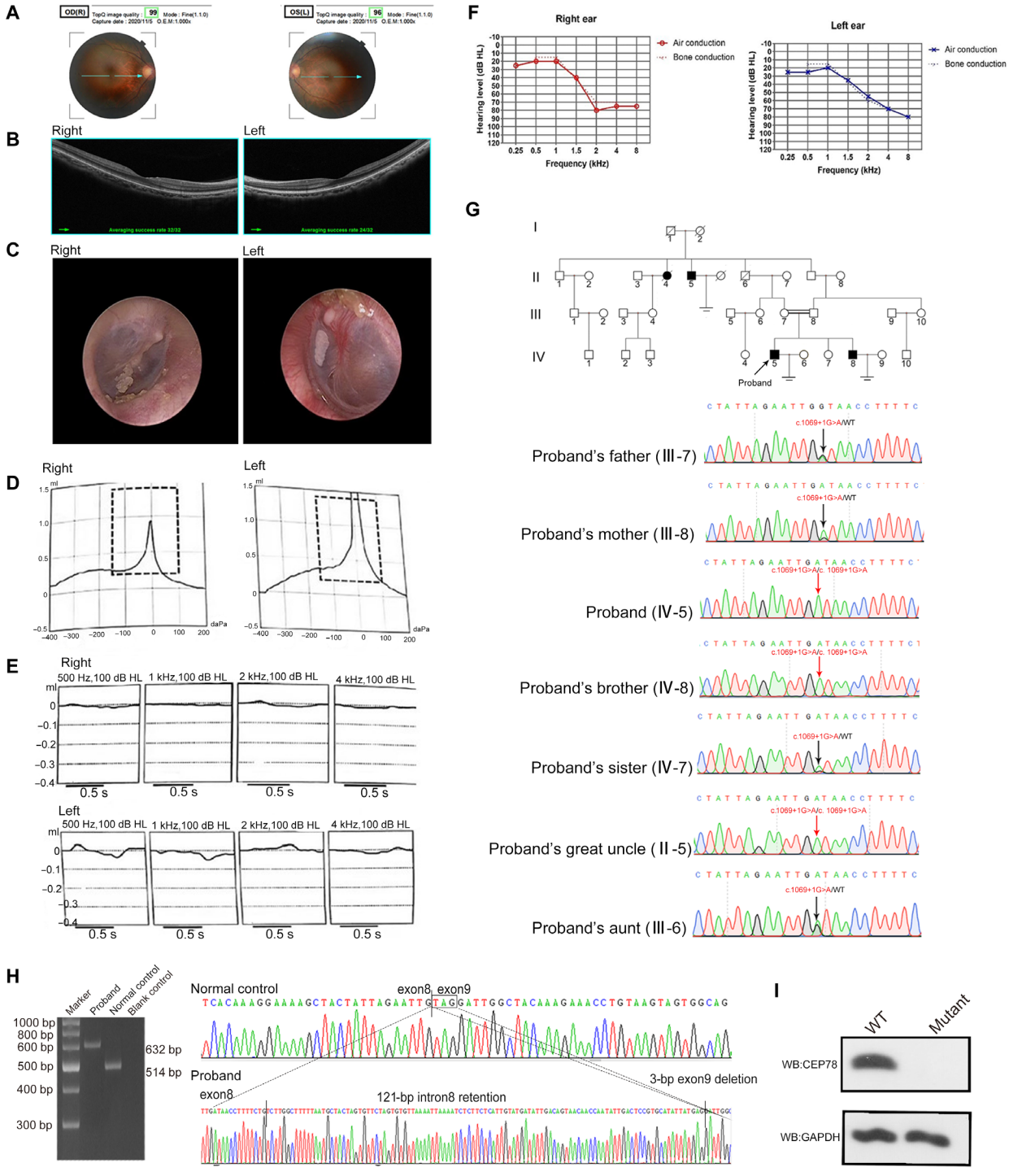

Fig. 1. A pathogenic splicing mutation in *CEP78* identified in an infertile family. (**A**) Color fundus photograph of the proband. The retina was generally normal except for tessellated fundus changes. (**B**) Optical coherence tomography results from the proband. The outer nuclear layer (ONL) appeared to be thinning, with the cone-rich macular fovea relatively preserved. The inner segment (IS)/outer segment (OS) layer was blurred. The extent of retinal changes between both eyes was similar. (**C**) Images of two-sided tympanic membranes observed in an otoscopic examination of the proband. (**D**) The acoustic immittance test results of the proband were shown on the right in an As-type picture and on the left as an A-type picture. (**E**) The acoustic reflection of the proband was not detected in the two ears. (**F**) Binaural pure-tone hearing threshold test results of the proband. (**G**) Pedigrees and sequence chromatograms of the identified mutation. The homozygotes are indicated by red arrows, and the heterozygotes are indicated by black arrows. (**H**) RT-PCR analysis was performed on cDNA samples from the proband (lane 2) and a normal control (lane 3). Lane 1 represents a DNA ladder. Lane 4 includes a blank control. Sanger sequencing showed aberrant integration of 121-bp bases of intron 8 and a 3-base deletion of exon 9 in the amplified cDNA fragment of the proband. Three independent experiments were performed. (**I**) Western blotting results showed that the mutant-*CEP78* plasmids did not result in CEP78 expression. Three independent experiments were performed. GAPDH, glyceraldehyde-3-phosphate dehydrogenase.

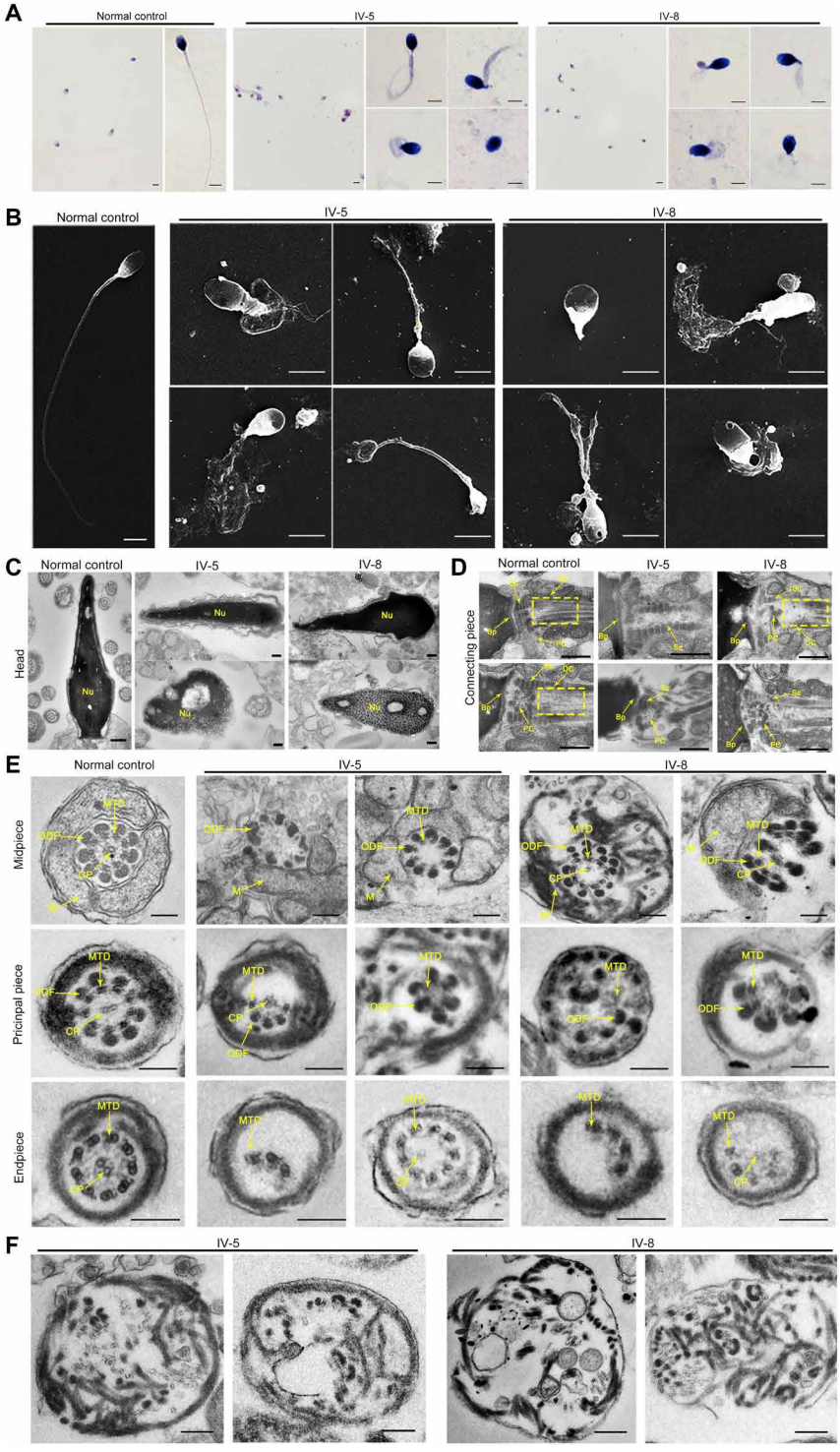

Fig. 2. Morphological and ultrastructural defects in spermatozoa from the two infertile siblings. (**A** and **B**) Papanicolaou staining (A) and scanning electron microscopy (SEM) (B) results showed various morphological abnormalities in sperm from the patients (scale bars, 5 μm). (**C**) Transmission electron microscopy (TEM) analyses showed the deformed sperm heads in samples from the siblings. Nu, nucleus (scale bars, 100 nm). (**D**) Aberrations in the sperm connecting piece detected in the siblings. Missing or defective proximal centrioles (PCs) and distal centrioles (DCs) were found. The dotted box denotes DC. Sc, segmented column; Bp, basal plate (scale bars, 100 nm). (**E**) In the patients' sperm flagella, ultrastructural abnormalities, including disorganized arrangements and/or absence of central-pair microtubules (CPs), peripheral microtubule doublets (MTDs), and outer dense fibers (ODFs), were observed using TEM. M, mitochondria; IV-5, the proband; IV-8, the affected sibling (scale bars, 100 nm). (**F**) TEM showed several flagellar pieces fused into a single piece wrapping numerous unorganized axoneme clusters in the sperm of the patients (scale bars, 100 nm).

spermatozoa; in mice, both CEP78 and centriole (marked by acetylated tubulin) staining were not observed in mature sperm, but they were colocalized in round spermatids (Fig. 3A and fig. S4A). We generated *Cep78* KO mice with a CRISPR-Cas9 system using a guide RNA (gRNA) targeting exons 2 through 4 to further investigate the role of *CEP78* in spermatogenesis (fig. S4, B and C). Immunofluorescence staining and Western blotting analysis further confirmed the successful establishment of the *Cep78* KO mice (Fig. 3A and fig. S4D). The *Cep78* KO mice were viable and showed no overt abnormalities, while the homozygous *Cep78* KO male mice exhibited complete infertility (fig. S4E). Although no detectable difference in the testis/body weight ratio was observed between WT and homozygous *Cep78* KO mice (fig. S4F), the number of homozygous *Cep78* KO spermatozoa collected from the cauda epididymis was reduced by approximately 90%, and all sperm were nearly completely immobile (fig. S4, G and H). To elucidate the etiology of infertility of the homozygous *Cep78* KO males, we examined the histology of *Cep78* KO tests and epididymis by performing hematoxylin and eosin (H&E) staining. Compared to the WT male mice, tissue sections from *Cep78* KO male mice showed that germ cells were sparsely arranged in the seminiferous tubules and the flagellar formation defects were evident during different spermatogenesis stages (fig. S5A). Fewer sperm cells were present in the lumen of epididymis (fig. S5B).

The results of the computer-assisted sperm analysis (CASA) also showed that, compared to WT male mice, the epididymal sperm count of homozygous *Cep78* KO male mice was obviously reduced and their sperm motility was substantially decreased, consistent with the patients' phenotype (Table 1 and movies S1 and S2). Light microscopy and SEM revealed severe morphological defects in spermatozoa from the homozygous *Cep78* KO mice, including absent, coiled, short, and irregular flagella and abnormal head shapes (Fig. 3, B and C, and fig. S6A). Moreover, TEM images of the homozygous *Cep78* KO spermatozoa showed evident chaos and absence of the axoneme and ODFs in the midpiece, and most of the principal piece exhibited missing CPs and disordered MTDs, as well as disorganized ODFs; MTDs were lacking in the end piece (Fig. 3D and fig. S6B). The amorphous sperm heads were well marked in most of the homozygous *Cep78* KO spermatozoa (Fig. 3E and fig. S6C). In addition, in homozygous *Cep78* KO spermatozoa, several flagellar pieces fused into a single piece with disordered axoneme clusters and ODFs (Fig. 3F), resembling the phenotype of patients carrying the *CEP78* variant. With abnormal development of the flagellar axoneme, altered mitochondrial distributions were detected using MitoTracker Red staining and TEM (fig. S7, A and B). Furthermore, TEM observations of the ultrastructure of spermatids from homozygous *Cep78* KO mice revealed defective PC during spermatogenesis, showing lacking or disarranged triplet microtubule; in addition, Sc was dysplasia, and arranged disorderly, while the development of Bp seemed normal (Fig. 3G). Collectively, CEP78 is essential for spermatogenesis, and its loss might lead to impairments in the centriole development of germ cells, causing male infertility related to aberrant sperm morphology and a diminished sperm count, as well as the disorganization of sperm ultrastructure, in both humans and mice.

Poor prognosis of ICSI treatment in patients carrying the *CEP78* variant and male *Cep78* KO mice

Intracytoplasmic sperm injection (ICSI) cycling was attempted for the proband, who signed an informed consent form for the ICSI procedure. The sperm DNA fragmentation index of the proband was in the normal range (17%, normal reference: ≤30%). The basal hormone data of the patient's wife were regular (Table 2). Ovulation was induced in her; a long protocol was presented in Table 2. Consequently, 13 oocytes were aspirated during follicular puncture, 10 of which were in metaphase II (MII). The ejaculated sperm from the patient were injected into 10 oocytes for ICSI cycling. As shown in Table 2, the cycle achieved a 60% fertilization rate, and four of the six embryos reached cleavage stages, but only one of them continued to develop and was blocked at the sixth cell stage on day 3 after ICSI. Sperm centrioles are essential for fertilization and early embryogenesis in humans and most nonmurine mammals (*25*, *26*), while patients with *CEP78* mutations exhibited evident defects in sperm centrioles. Thus, we speculated that *CEP78* mutations resulting in aberrant sperm centrioles might be the main cause of low fertilization rates and unsuccessful embryonic development during ICSI treatment.

As expected, the infertility of homozygous *Cep78* KO male mice was also not overcome through ICSI. Coincidentally, the rates of zygotes, two-cell embryos, and blastocysts were markedly lower in the group using spermatozoa from homozygous *Cep78* KO male mice than in those using spermatozoa from WT male mice. As shown in Fig. 4, the fertilization rates, two-cell rates, and blastocyst rates of the *Cep78* KO group were 46.28, 37.50, and 5.62%, respectively, while those of the WT group were 82.10, 64.95, and 34.69%, respectively. Unlike humans, mouse sperm centrioles may not be present within the zygote and play an irrelevant role in fertilization and embryonic development (*26*). We subsequently assessed other factors that might be related to the failed fertilization and embryogenesis in *Cep78* KO mice. Sperm DNA fragmentation, a marker of DNA damage, has been suggested to be associated with reduced fertilization and pregnancy rates, poor embryo quality, and increased miscarriage rates (*27*). However, no obvious DNA fragments in the sperm were observed in *Cep78* KO mice (fig. S8, A and B). Micronuclei are small, extranuclear chromatin bodies surrounded by a nuclear envelope, indicating clastogenic and aneugenic chromosomes that are related to failed embryonic development (*28*, *29*). However, no obvious micronuclei staining was observed in the embryos from both *Cep78* KO mice and WT mice (fig. S8, C and D). We therefore suggested that the loss of CEP78 expression might disrupt the function of several key molecules (see below) that are essential for fertilization and embryogenesis and then lead to unsuccessful ICSI treatment in *Cep78* KO mice. Collectively, these findings indicated that CEP78 plays important biological roles in fertilization and early embryonic development in humans and mice.

CEP78 regulates USP16-mediated Tektin function in spermatogenesis

To explore the mechanism behind CEP78 regulating spermatogenesis, we used a proteomics approach on testes from WT mice and homozygous *Cep78* KO mice. A total of 5367 proteins were quantified, including 90 up-regulated proteins and 237 down-regulated proteins (fig. S9). Gene Ontology (GO) enrichment analysis demonstrated obviously altered categories of proteins in response to *Cep78* deletion. The down-regulated proteins were associated with flagellogenesis and ciliogenesis along with other processes involved in spermatogenesis, such as meiosis I, spermatid differentiation, acrosomal vesicle, and so on (Fig. 5A). The up-regulated proteins were enriched for the GO terms related to the apoptotic pathway in *Cep78* KO mice (Fig. 5B). Among the down-regulated proteins, 34 were involved in ciliogenesis, 16 participated in fertilization and embryonic

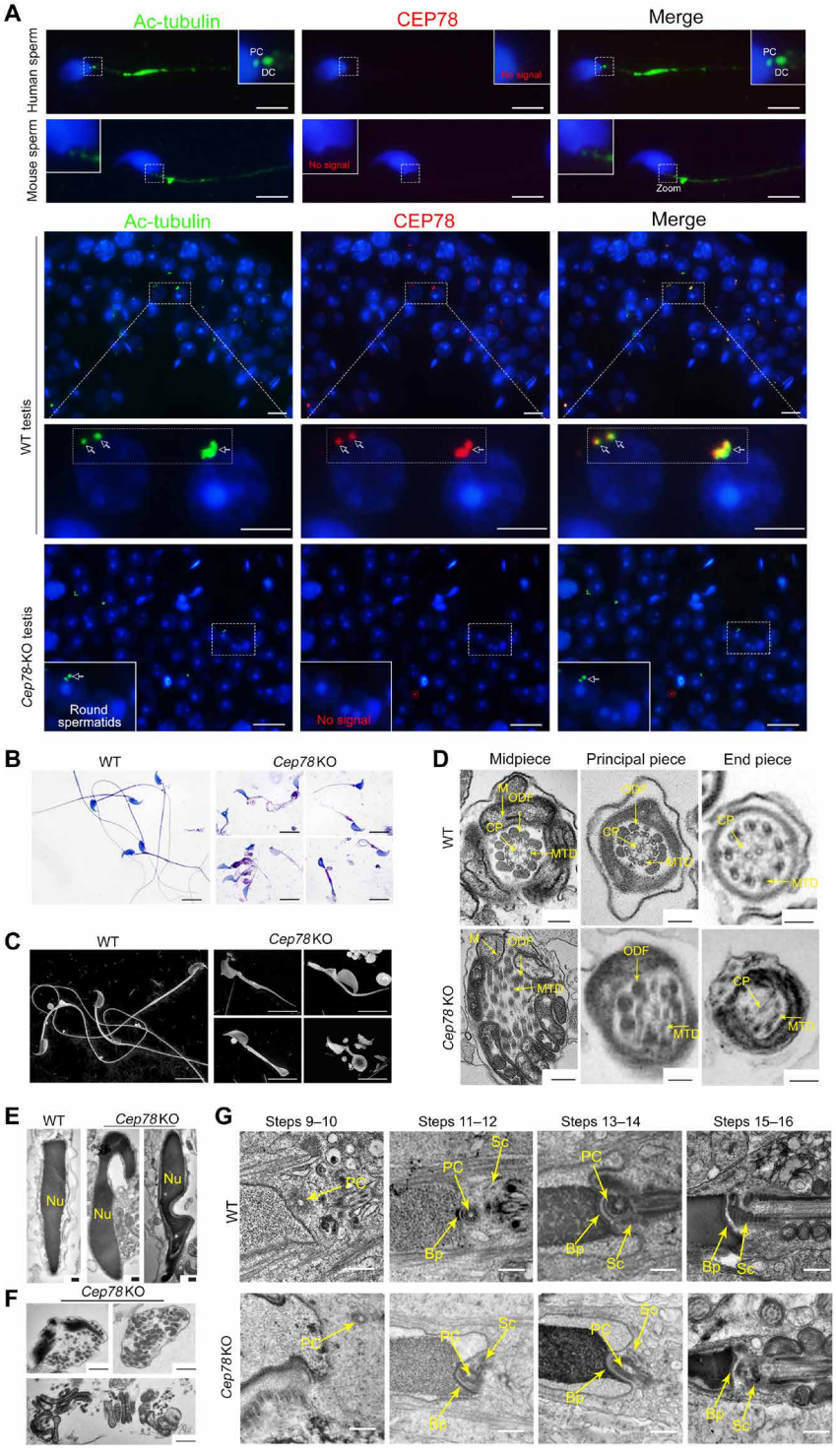

Fig. 3. Impaired spermiogenesis in male homozygous *Cep78* KO mice. (**A**) Immunofluorescence staining showing that CEP78 was not detectable in mature spermatozoa of humans and mice or in *Cep78* KO testes. Ac-tubulin (labeling centrioles) staining was defective in *Cep78* KO testes ($n = 3$ biologically independent WT mice or KO mice; scale bars, 10 μm). (**B** and **C**) Light microscopy (B) and SEM (C) showed that spermatozoa from *Cep78* KO mice manifested aberrant flagellar morphologies, including short, coiled, bent, and irregular flagella ($n = 3$ biologically independent WT mice and KO mice; scale bars, 10 μm). (**D**) TEM showed disorganized or absent ODFs, MTDs, and CPs in *Cep78* KO mouse spermatozoa ($n = 3$ biologically independent WT mice and KO mice; scale bars, 200 nm). (**E**) The spermatozoa head showed irregular shapes in *Cep78* KO mice. ($n = 3$ biologically independent WT mice and KO mice; scale bars, 200 nm). (**F**) A number of unorganized axoneme clusters from different flagellar pieces were mixed into a single piece in *Cep78* KO mice ($n = 3$ biologically independent WT mice and KO mice; scale bars, 200 nm). (**G**) Impaired development of sperm connecting piece during spermiogenesis in *Cep78* KO mice, showing defective PC and Sc, and seemingly normal Bp ($n = 3$ biologically independent WT mice and KO mice; scale bars, 500 nm).

Table 1. Semen analysis using CASA in the mouse model of *Cep78* KO.
n = 3 biologically independent WT mice or KO mice.

	Adult male mice		
	WT	KO	*P**
Semen parameters			
Sperm concentration (10^6/ml)†	39.80 ± 4.32	4.57 ± 2.32	<0.001
Motility (%)	75.14 ± 2.23	2.11 ± 1.10	<0.001
Progressive motility (%)	71.77 ± 1.13	1.20 ± 0.90	<0.001
Sperm locomotion parameters			
Curvilinear velocity (VCL) (μm/s)	121.17 ± 9.32	6.50 ± 3.37	<0.001
Straight-line velocity (VSL) (μm/s)	50.17 ± 6.59	1.17 ± 0.21	<0.001
Average path velocity (VAP) (μm/s)	65.67 ± 3.22	3.21 ± 1.97	<0.001
Amplitude of lateral head displacement (ALH) (μm)	1.30 ± 0.15	0.14 ± 0.08	<0.001
Linearity (LIN)	0.41 ± 0.08	0.04 ± 0.03	0.002
Wobble (WOB, = VAP/VCL)	0.59 ± 0.07	0.21 ± 0.06	0.002
Straightness (STR, = VSL/VAP)	0.76 ± 0.12	0.29 ± 0.09	0.006
Beat-cross frequency (BCF) (Hz)	5.97 ± 0.055	0.42 ± 0.12	<0.001

*Two-sided Student's *t* test. †Epididymides and vas deferens.

Table 2. Clinical features of the patient's wife with ICSI treatment.
FSH, follicle-stimulating hormone; LH, luteinizing hormone; E2, estradiol; PRL, prolactin; Prog, progesterone; Testo, testosterone.

Age (years)		27
Length of primary infertility history (years)		7
Body mass index		19.7
Basal hormones	FSH (IU/liter)	3.6
	LH (IU/liter)	1.5
	E2 (pg/ml)	47.5
	PRL (ng/ml)	8.8
	Prog (ng/ml)	0.31
	Testo (ng/ml)	0.2
Cycle 1	Protocol	Long
	E2 level on the trigger day (pg/ml)	6034.7
	No. of follicles ≥14 mm on the trigger day	11
	No. of follicles ≥18 mm on the trigger day	7
	No. of oocytes retrieved	13
ICSI progress	Oocytes injected	10
	Fertilization rate (%)	60% (6/10)
	Cleavage rate (%)	66% (4/6)
	Six-cell formation rate (%)	25% (1/4)
	Eight-cell formation rate (%)	0
	Blastocyst formation rate (%)	0

development, 19 were related to spermatogenesis, 25 were associated with flagellogenesis, and 13 were involved in sperm head development (Fig. 5C). Specifically, among the reduced proteins involved in fertilization and embryonic development, deficiencies in basigin (Bsg), DNA-damage inducible protein 2 (DDI2), HYLS1 centriolar and ciliogenesis associated (Hyls1), NIMA related kinase 2 (Nek2), pumilio RNA-binding family member 1 (Pum1), DNA topoisomerase I (Top-1), serine (or cysteine) peptidase inhibitor, clade A, member 1A (Serpina1a), abhydrolase domain containing 2 (Abhd2), cation channel sperm associated 2 (CatSper2), and Spata3 have been suggested to lead to unsuccessful fertilization or embryogenesis in mice (*30*–*39*). We thus suggested that the failure in ICSI treatment of *Cep78* KO mice might be because the loss of CEP78 impairs the expression of these key molecules linked to fertilization and early embryonic development. Moreover, the interaction of the differentially expressed proteins, which have been reported to play important roles in reproductive processes in humans and/or mice, between *Cep78* KO mice and WT mice was analyzed using a network diagram, and the results indicated that proteins involved in these processes had complex interactions (Fig. 5D). Among the 237 down-regulated proteins, we focused on the distinctly reduced expression of Tektin family members, including Tektin 1 (TEKT1), TEKT2, TEKT3, TEKT4, and TEKT5, for the reasons described below: (i) Among the down-regulated proteins in the top 25 differentially expressed proteins, eight proteins, including TEKT2, TEKT3, TEKT5, testis, prostate, and placenta expressed (Tepp), spermatid-specific manchette-related protein 1 (Smrp1), testis expressed 43 (Tex43), late cornified envelope like proline rich 1 (Lelp1), tubulin polymerization promoting protein family member 2 (Tppp2), and outer dense fiber of sperm tails 3 (Odf3), were predominantly expressed in the testis. (ii) According to the literature, the loss of TEKT2 in male mice leads to a deficiency in flagellar construction and produces immotile sperm (*40*). Sperm from *Tekt3*$^{-/-}$ male mice show reduced motility and an increase in flagellar structural defects (*41*). The TEKT5 protein is enriched in flagellar accessory structures (*42*). These reports of roles for Tektins in sperm flagella formation consequently showed a strong association with the aberrant sperm flagella identified in our patients and *Cep78* KO mice. (iii) The remaining five proteins are not suggested to play a role in spermatogenesis. (iv) We also detected sharply reduced expression of TEKT1 and TEKT4 in the down-regulated proteins out of the top 25 differentially expressed proteins; importantly, TEKT1 is suggested to participate in the nucleation of the flagellar axoneme of spermatozoa and is also proposed to be involved in acrosome-related phenomena (*43*, *44*). The absence of TEKT4 causes asthenozoospermia associated with markedly reduced sperm motility and subtle disorganization of the flagellar ultrastructure in male mice (*45*). Therefore, TEKT1 and TEKT4 deficiencies might also be linked to the phenotype of the patients and *Cep78* KO mice. (v) Tektins are expressed in the centrioles and basal bodies of the male germ cell lineage (*46*), and CEP78 is a centriole wall protein that

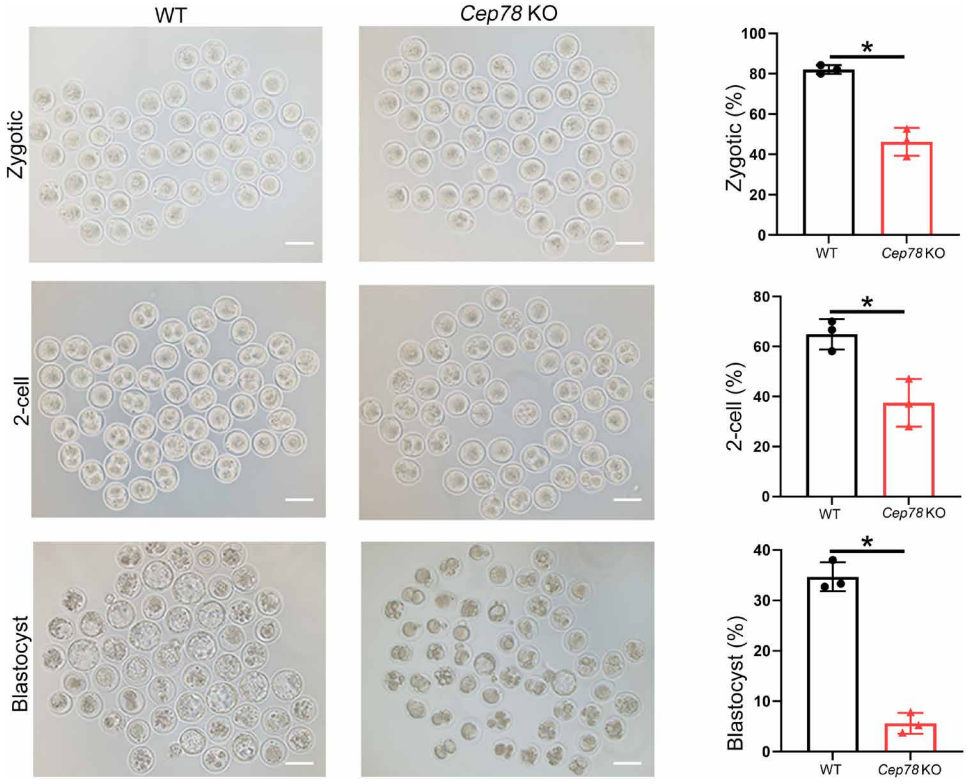

Fig. 4. ICSI treatment using the sperm from *Cep78* KO mice led to poor outcomes. Representative zygotic embryos, two-cell embryos, and blastocysts obtained from ICSI treatment in mice. Obviously reduced percentages of zygotic embryos, two-cell embryos, and blastocysts were observed in the *Cep78* KO group ($n = 3$ biologically independent WT mice and KO mice; scale bars, 100 μm; two-sided Student's *t* test; $^*P < 0.05$; error bars, SEM).

is detected in spermatid centrioles; these proteins localize in the germ cell centrioles, thus indicating that Tektins and CEP78 might interact during spermatogenesis. Therefore, we hypothesized that CEP78 might be involved in the Tektin functional pathway during spermatogenesis.

Western blotting and immunofluorescence staining confirmed the decreased expression of Tektin family members in the homozygous KO mice compared to the WT mice, consistent with the tandem mass tag (TMT) quantification results (Fig. 5, E and F, and fig. S10A). We aimed to confirm that the reduction in Tektins is due to CEP78 deficiency but not the defects of sperm, and observed the down-regulation of these molecules in hRPE1 cells transfected with a short hairpin RNA (shRNA) against *CEP78* (fig. S10B). We further explored the expression of Tektins during spermatogenesis in humans and mice (figs. S11 and S12). Immunofluorescence staining of germ cells in different stages showed that TEKT1 and TEKT4 were localized in the heads and flagella of various spermatids. TEKT2 and TEKT5 were predominantly expressed in the cytoplasm of different spermatids during spermatogenesis. TEKT3 was not only expressed in the tails of elongating spermatids but also mainly expressed in the heads of spermatids.

Cep78 binds specifically to EDD-DYRK2-DDB1^{VprBP} and inhibits its activity to mediate the ubiquitination of centriolar coiled coil protein 110 kDa (CP110), thereby regulating centriole length and cilia assembly (*47*). We thus hypothesized that CEP78 might regulate Tektin abundance via ubiquitination pathway. As expected, increased ubiquitination and degradation of Tektins was observed in the KO mice compared to the WT mice (Fig. 5G). To understand the mechanism of CEP78 inhibiting the ubiquitination and degradation of Tektins, we analyzed the differentially expressed E3 ubiquitin ligases or deubiquitinating enzymes between the KO and WT mice. Last, among the identified differentially expressed proteins, only two reduced deubiquitinating enzymes were detected: USP16/USP21 and MINDY lysine 48 deubiquitinase 2 (MINDY2). MINDY2 is predicted to be involved in protein K48-linked deubiquitination, but intriguingly, USP16 is involved in centrosome- and microtubule-associated functions (*48*), indicating a potential relationship between USP16 and CEP78. We then confirmed a greater reduction in USP16 expression in the testes of KO mice than in those of WT mice using Western blotting and immunofluorescence staining (Fig. 5, E and H). The spatiotemporal expression of USP16 in spermatogenic cells from humans and mice indicated that USP16 might play a role in spermatogenesis (fig. S13). Collectively, CEP78 might play a role in spermatogenesis by regulating USP16 expression to subsequently inhibit the ubiquitin-mediated degradation of Tektins. In addition, we identified and confirmed a marked decrease in the levels of H1.7 linker histone (H1-7), a haploid germ cell–specific nuclear protein, whose deficiency causes defects in sperm nuclear formation (*49*), in *Cep78* KO mice (Fig. 5, E and H). Thus, we speculated that the aberrant sperm heads observed in *Cep78* KO mice might be attributed to the reduced H1-7 expression due to *Cep78* deletion. Moreover, the observation that H1-7 was mainly expressed in the nuclei of germ cells of humans and mice (fig. S14) supported the concept that H1-7 is crucial for sperm head formation. We first checked that the transcript level of *H1-7* was not largely affected by *Cep78*

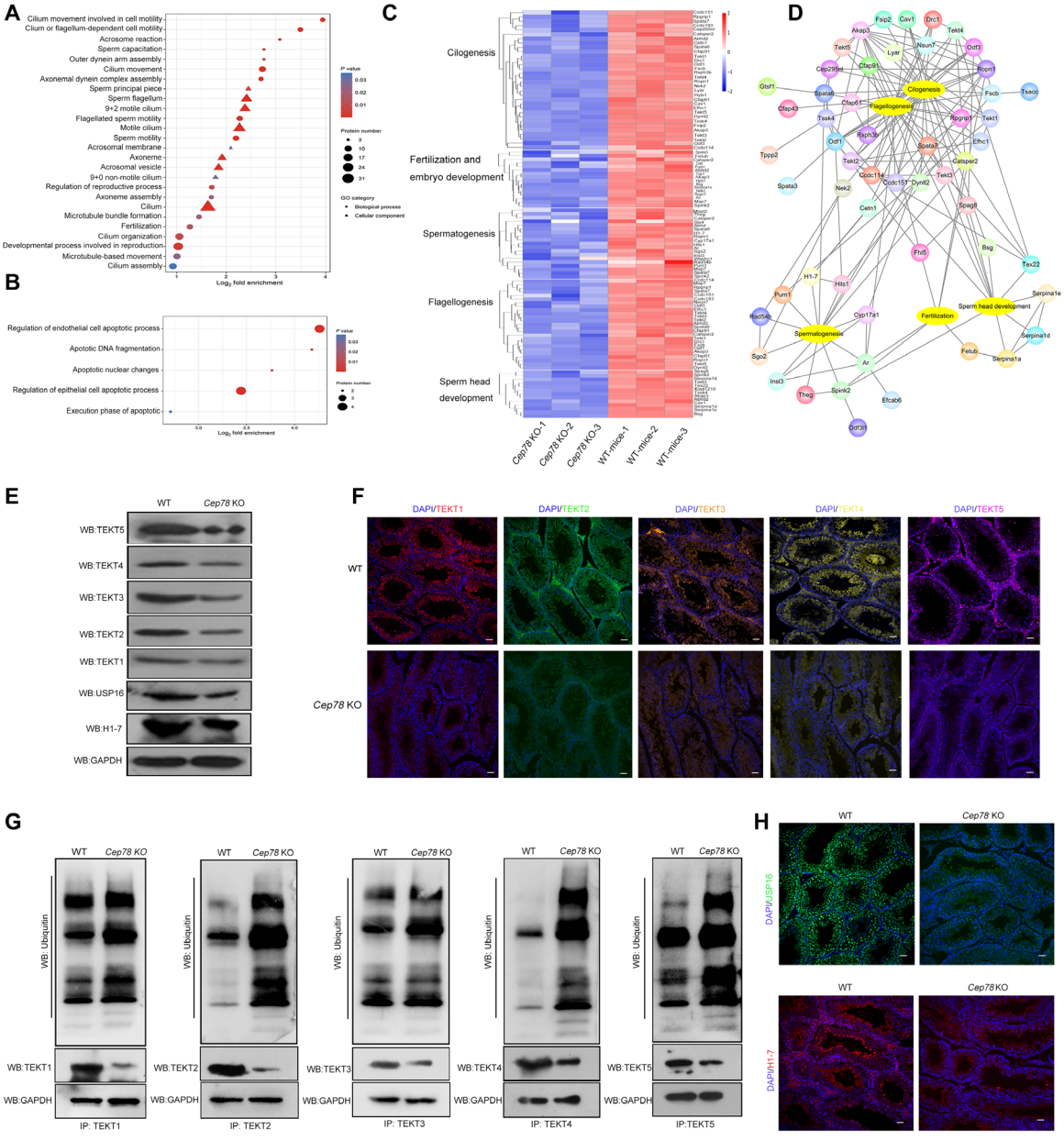

Fig. 5. Effect of CEP78 on spermatogenesis by regulating USP16-mediated Tektin function. (**A**) Bubble chart showing the decreased enrichment of proteins related to spermatogenetic process according to the GO analysis of *Cep78* KO mouse testes compared to WT mouse testes. (**B**) GO analysis showed an up-regulated apoptotic process in *Cep78* KO mice compared to WT mice. (**C**) Heatmap showing differentially enriched proteins in the testes of *Cep78* KO mice and WT mice. The down-regulated proteins were mainly involved in ciliogenesis, fertilization and embryo development, spermatogenesis, flagellogenesis, and sperm head development. (**D**) Interaction network of down-regulated proteins in *Cep78* KO mice. (**E**) Western blotting assays confirmed the decreased expression of H1-7, USP16, and Tektins identified by the proteomic analysis in *Cep78* KO mice compared to WT mice ($n = 3$ biologically independent WT mice or KO mice). (**F**) Immunostaining indicated the decreased Tektin expression in testis sections from *Cep78* KO compared to WT mice ($n = 3$ biologically independent WT mice or KO mice; scale bars, 125 μm). (**G**) Increased ubiquitination of Tektins in the testes of *Cep78* KO mice compared to those in WT mice ($n = 3$ biologically independent WT mice and KO mice). (**H**) Decreased levels of the USP16 and H1-7 proteins detected using immunofluorescence staining in the testes of KO mice compared to those in WT mice ($n = 3$ biologically independent WT mice and KO mice; scale bars, 125 μm).

depletion in mouse testes (fig. S15A). The different localizations of CEP78 (centriole) and H1-7 (nucleus), however, suggested that CEP78 might not regulate H1-7 expression directly but by a mediating molecule. We further noticed the interaction of H1-7 and CETN1 in the network diagram (Fig. 5D), and their binding was next confirmed in mouse testes by a co-immunoprecipitation (Co-IP) assay (fig. S15B). Notably, CETN1 localized to both the nucleoplasm and centriolar satellite (https://proteinatlas.org/ENSG00000177143-CETN1/subcellular), indicating that CEP78 might regulate H1-7 expression through the mediator CETN1. Because of no available cell line expressing CETN1, we only validated the reduced CETN1 expression in *Cep78* KO mice compared to WT mice (fig. S15C).

Moreover, a Co-IP assay confirmed the interaction of CEP78 and CETN1 in mouse testes (fig. S15D). Thus, CEP78 might indirectly regulate H1-7 expression by mediating CETN1.

CEP78 interacts with USP16 to suppress Tektin ubiquitination and degradation

To elucidate in detail the molecular mechanism of CEP78 conducting Tektin expression via its interaction with USP16, we first confirmed that CEP78 directly affects USP16 abundance. hRPE1 cells were transfected with *CEP78* shRNA, and Western blotting revealed that CEP78 knockdown reproducibly reduced the level of endogenous USP16 (Fig. 6A). Moreover, a more marked increase in the USP16 level was observed in the 293T cells overexpressing CEP78 (fig. S16A). We determined whether the effects on USP16 stability resulting from changes in CEP78 expression were due to an interaction between endogenous CEP78 and USP16 by detecting this interaction using antibodies against USP16 or CEP78 (Fig. 6B). On the basis of these results, the USP16 abundance may be regulated by its interaction with CEP78.

Increased ubiquitination and degradation of Tektins (TEKT1, TEKT2, TEKT3, TEKT4, and TEKT5) was observed in *Cep78* KO mice compared to WT mice (Fig. 5G). USP16 is a deubiquitinase associated with both centrosome and microtubule functions, and that contributes to inducible gene expression (*48*). To determine whether Tektin expression is regulated by deubiquitinating enzyme activity, hRPE1 cells were treated with PR-619, a deubiquitinating enzyme inhibitor, for 8 hours. Western blotting revealed that the Tektin abundance was markedly decreased in cells treated with increasing concentrations of PR-619 (Fig. 6C). Thus, the degradation of Tektins was actively prevented by deubiquitinating enzyme.

We further confirmed that Tektins were down-regulated by knocking down USP16 in hRPE1 cells (Fig. 6D). In addition, ectopic expression of USP16 markedly increased Tektin abundance in 293T cells (Fig. 6E). The interactions of USP16 with Tektins were confirmed in mouse testis (fig. S16, B and C). To confirm that the effects of USP16 knockdown on Tektin expression are mediated by proteasomal degradation, hRPE1 cells transfected with an shRNA targeting *USP16* (sh*USP16*) were treated with the proteasome inhibitor MG132. Western blotting consolidated that Tektin destabilization resulting from USP16 knockdown was partially rescued by proteasome inhibition (Fig. 6F). Furthermore, we analyzed the influence of USP16 on Tektin ubiquitination and found that the down-regulation of USP16 markedly enhanced the ubiquitination of endogenous Tektins (Fig. 6G). In contrast, overexpression of USP16 showed remarkable inhibition of Tektin ubiquitination (Fig. 6H); therefore, USP16 directly binds and deubiquitinates Tektins. Collectively, we suggested that CEP78 might control USP16 expression to stabilize the sperm-connecting piece and to mediate ubiquitination and proteasome-mediated degradation of Tektins during flagellogenesis, as well as regulating sperm head formation by modulating CETN1-mediated H1-7 expression; meanwhile, the loss of CEP78 function impairs the expression of key molecules in the involvements of early embryonic development, resulting in the unsuccessful ICSI treatment in *Cep78* KO mice (Fig. 6I).

CEP78 variants detected in infertile males

Although our findings from human and mouse experiments unveiled a pivotal role for CEP78 in male reproduction, the frequency of *CEP78* variants in a sporadic male sterile population remains unclear. Therefore, we screened *CEP78* variations in 473 infertile individuals, including 7 with cryptozoospermia, 248 with oligoasthenoteratozoospermia, and 218 with azoospermia, using multiplex PCR. Noticeably, six heterozygous *CEP78* variants, including one frameshift variant and five missense variants, were observed in five patients with oligoasthenoteratozoospermia and one patient with azoospermia, respectively. The allele frequencies of these variants were quite low or absent in the public databases, and the pathogenicity of these variants was supported by bioinformatics tools (Table 3). In addition, neither heterozygosity nor homozygosity of these variants was detected in our 1000 normal Chinese control males. Although no homozygous *CEP78* variants were identified in our 473 unrelated infertile individuals, the rare deleterious heterozygous *CEP78* mutations were only detected in these patients but not the normal control, suggesting that heterozygous *CEP78* mutations might be the guest players for male infertility.

Retinal degeneration and impaired function of OHCs detected in homozygous *Cep78* KO mice

Although *CEP78* mutations lead to cone-rod degeneration in humans, the role of *Cep78* in retinal development in mice is unexplored. To evaluate the physiological role of *Cep78* in the retina in mice, we analyzed the retina function of *Cep78* KO mice and WT mice at different ages. We initially found that the composition of the retina in *Cep78* KO mice and WT mice was similar by performing a histological analysis (Fig. 7A). We then further measured the thickness of the ONL, and the results showed no obvious change in the ONL thickness between *Cep78* KO mice and WT mice of different ages (Fig. 7B), whereas the lengths of the IS and OS were markedly shortened in 6-month-old *Cep78* KO mice compared to WT mice (Fig. 7C). At 1 month of age, the retina showed no obvious abnormalities using CFP, immunofluorescence staining for peanut agglutinin (PNA) (labeling cones) and rhodopsin (labeling rods), or electroretinography (ERG) in *Cep78* KO mice (Fig. 7, D to F). In *Cep78* KO mice, at the age of 3 months, the CFP test showed grayish retinal pigment mottling, similar to the appearance of retinitis pigmentosa (Fig. 7D). On the basis of the results of immunofluorescence staining, the rods labeled with rhodopsin antibody in the OS were shorter in length, and the number of cones labeled with PNA antibody decreased (Fig. 7E). During the full-field ERG examination of mice of this age, a marked reduction in amplitude of the b-wave was recorded following light adaptation, but a slight reduction in dark adaptation was observed, indicating compromised cone function (Fig. 7F). Moreover, at the age of 6 months, atrophy lesions were scattered in the CFP of *Cep78* KO mice (Fig. 7D), and rhodopsin and PNA were rarely detected in these lesions (Fig. 7E). In addition, the amplitudes of the light-adaptive b-wave and dark-adaptive a-wave and b-wave were reduced (Fig. 7F). These findings suggested that the absence of *Cep78* causes a progressive loss of retinal function in mice.

We further investigated the expression of several proteins that are critical for the function of cones [G protein–coupled receptor kinase 1 (GRK1)], rods [phosphodiesterase 6B, PDE6b and receptor accessory protein 6 (REEP6)], and OS [scoliosis, idiopathic, susceptibility to, 4 (IS4)] in *Cep78* KO mice. Reduced expression of these proteins was evident in *Cep78* KO mice compared to WT mice (Fig. 7G). As we suggested a crucial role for CEP78 in the spermatogenic process by regulating Tektin expression, we next investigated the expression of TEKT1, TEKT2, TEKT3, and TEKT4 in the retinas of *Cep78* KO mice at the age of 6 months. Notably, we observed

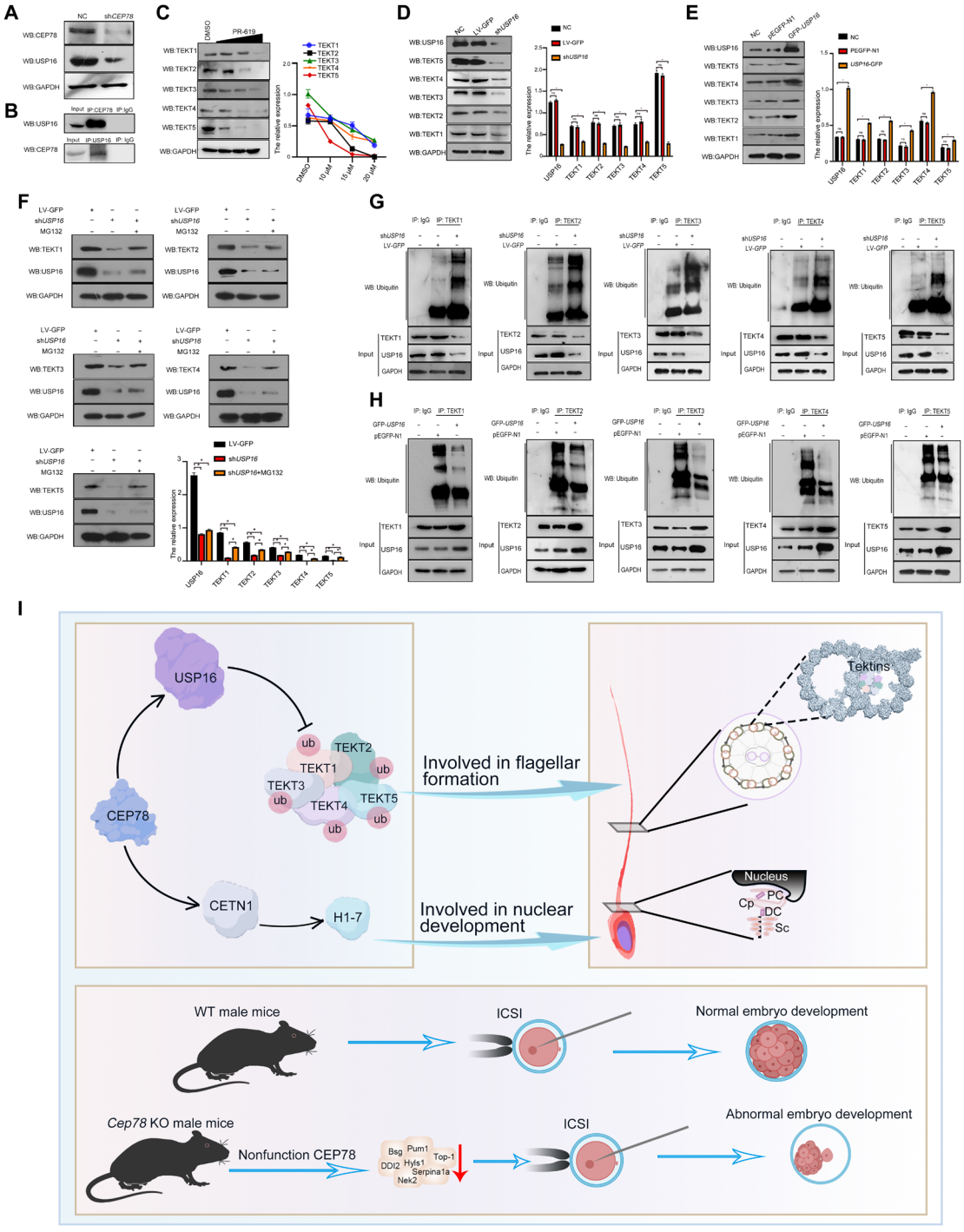

Fig. 6. CEP78 suppresses Tektin ubiquitinated degradation by interacting with USP16. (**A**) Western blotting showed that CEP78 down-regulation decreased the USP16 expression. NC, negative control. (**B**) Co-immunoprecipitation assay of endogenous CEP78 and USP16 using mouse testis lysates. IgG, immunoglobulin G. (**C**) Western blotting showing that Tektin expression was reduced as the PR-619 concentration was elevated. DMSO, dimethyl sulfoxide (error bars, SEM). (**D**) Western blotting showing that the Tektin down-regulation resulted from the decreased USP16 expression (two-sided Student's *t* test; **P* < 0.05; ns, no significance; error bars, SEM). GFP, green fluorescent protein. (**E**) Western blotting showing that the up-regulated USP16 increased Tektin expression (two-sided Student's *t* test; **P* < 0.05; error bars, SEM). (**F**) The degradation of Tektins resulting from knockdown of USP16 was rescued by MG132 treatment (two-sided Student's *t* test; **P* < 0.05; error bars, SEM). (**G**) Western blotting showed that the down-regulated USP16 contributed to the increased ubiquitination levels of Tektins. (**H**) Western blotting showing that the overexpressed USP16 led to the reduced ubiquitination levels of Tektins. (**I**) Proposed model for the mechanisms of action underlying the involvement of CEP78 in spermatogenesis and embryo development. CEP78 plays a role in sperm-connecting piece formation by up-regulating USP16 expression, and this increase in USP16 expression inhibits ubiquitin-mediated degradation of Tektins to regulate the biogenesis of sperm flagella. Loss of CEP78 protein also suppresses the normal functioning of proteins essential for embryogenesis, which further leads to the failed ICSI treatment in *Cep78* KO mice. Three independent experiments were performed.

Table 3. Analysis of *CEP78* mutations in infertile males. NA, not available.

	Human subjects				
	2016036 2017039 PS1903	**2016090**	**2016223**	**2018018**	**PS2120**
Phenotype	Oligoasthenoteratozoo-spermia	Oligoasthenoteratozoo-spermia	Oligoasthenoteratozoo-spermia	Azoospermia	Oligoasthenoteratozoo-spermia
cDNA mutation*	c.710A>G (rs186712872)	c.1345_1346del	c.1797C>G (rs778991962)	c.2015C>T (rs770261747)	c.1738G>C
Genotype	Heterozygous	Heterozygous	Heterozygous	Heterozygous	Heterozygous
Protein alteration	p.N237S	p.V449fs	p.I599M	p.P672L	p.A580P
Mutation type	Missense	Frameshift	Missense	Missense	Missense
Allele frequency in ExAC	0.0003	0	0.00003366	0.00004433	0
1000G project	0.000599042	0	0	0	0
gnomAD	0.0003	0	0.00001184	0.00006535	0
Function prediction					
SIFT	Deleterious	NA	Deleterious	Deleterious	Deleterious
PolyPhen-2	Probably damaging	NA	Probably damaging	Probably damaging	Possibly damaging
Mutation Taster	Disease_causing	NA	Polymorphism	Disease_causing	Polymorphism

*The GenBank accession number for *CEP78* is NM_001098802.

aberrant expression of these four proteins in *Cep78* KO mice (Fig. 7G). Thus, Tektins might also play a role in retinal function.

Given that *CEP78* mutations lead to hearing loss in humans, we further investigated the hearing function of *Cep78* KO mice. The auditory brainstem response (ABR) is currently the most mature and commonly used auditory electrophysiological test and reflects the complete function and loss of the auditory pathway from the outer ear to the lower brainstem. Techniques for ABR testing in mice include click-ABR and tone-burst ABR; the former is used to evaluate broadband hearing, and the latter is used to test hearing loss at each frequency separately. The ABR threshold of *Cep78* KO mice at the age of 1 month did not exceed 30 dB sound pressure level (SPL), which was within the normal range (Fig. 7H, a). At the age of 3 months, the click-ABR threshold of *Cep78* KO mice was 30 dB SPL, and the tone-burst ABR thresholds at 4, 8, 16, and 32 kHz were 55, 50, 55, and 50 dB SPL, respectively, indicating moderate to severe sensorineural hearing loss (Fig. 7H, a). Moreover, the click-ABR threshold of *Cep78* KO mice at the age of 6 months was 45 dB SPL, and the tone-burst ABR at 32 kHz was 55 dB SPL, which indicated more severe hearing loss than in 3-month-old *Cep78* KO mice (Fig. 7H, a). The distortion product otoacoustic emissions (DPOAE) test measures the spontaneous discharge function of cochlear OHCs to assess the integrity of cochlear OHC function and hearing. Therefore, we subsequently performed a DPOAE test on *Cep78* KO mice of different ages. The DPOAE responses of the 1-month-old *Cep78* KO mice at each test frequency were all elicited, and the elicitation threshold did not exceed 20 dB SPL, which is a normal hearing performance range (Fig. 7H, b). DPOAE responses were all elicited at the frequencies of 4, 8, 16, and 32 kHz in 3-month-old *Cep78* KO mice, with average thresholds of 20, 30, 25, and 25 dB SPL (Fig. 7H, b), respectively, indicating hearing loss in the 3-month-old *Cep78* KO mice. The 6-month-old *Cep78* KO mice did not elicit DPOAE responses at each frequency at the maximum stimulus intensity, suggesting the poor function of OHCs and hearing loss exceeding 50 dB SPL (Fig. 7H, b). Collectively, the auditory function of *Cep78* KO mice showed progressive damage.

DISCUSSION

Although previous studies suggest that *CEP78* loss-of-function mutations cause CRDHL syndrome in humans, the roles of CEP78 in mouse vision and hearing, as well as in male infertility in humans and mice, have not been documented. In the present study, we identified an unreported *CEP78* splicing mutation in patients with oligoasthenoteratozoospermia, and by creating *Cep78* KO mice, we demonstrated that loss-of-function mutations in *CEP78*/*Cep78* directly contribute to male infertility. We also suggested that CEP78 might play a role in spermatogenesis by promoting USP16-mediated modulation of Tektin expression via ubiquitin signaling. Moreover, we revealed that *Cep78* deficiency results in abnormal vision and hearing in mice. Thus, our work identifies a function for CEP78 in human and mouse genetics and reveals a potential mechanism regulating spermatogenesis.

To date, several inactivating variants, a missense variant, and two complex structural variants in *CEP78* have been identified in individuals with autosomal recessive CRDHL syndrome, a rare syndromic inherited retinal disease accompanied by sensorineural hearing loss (*19*–*22*). In addition, two splicing mutations in *CEP78* were identified in two independent families with a mild degree of Usher syndrome, a genetic disorder characterized by the combination of retinitis pigmentosa and sensorineural hearing loss (*50*). One of these reports suggested that *CEP78* mutations might also be correlated with reduced male infertility (*21*). Inexplicably, in that study, two patients with CRDHL syndrome carried the same mutation of *CEP78* (c.449T>C, p.Leu150Ser, NM_001098802.1), while one (F1, III-2) was infertile and another had offspring (F2, II-2); in

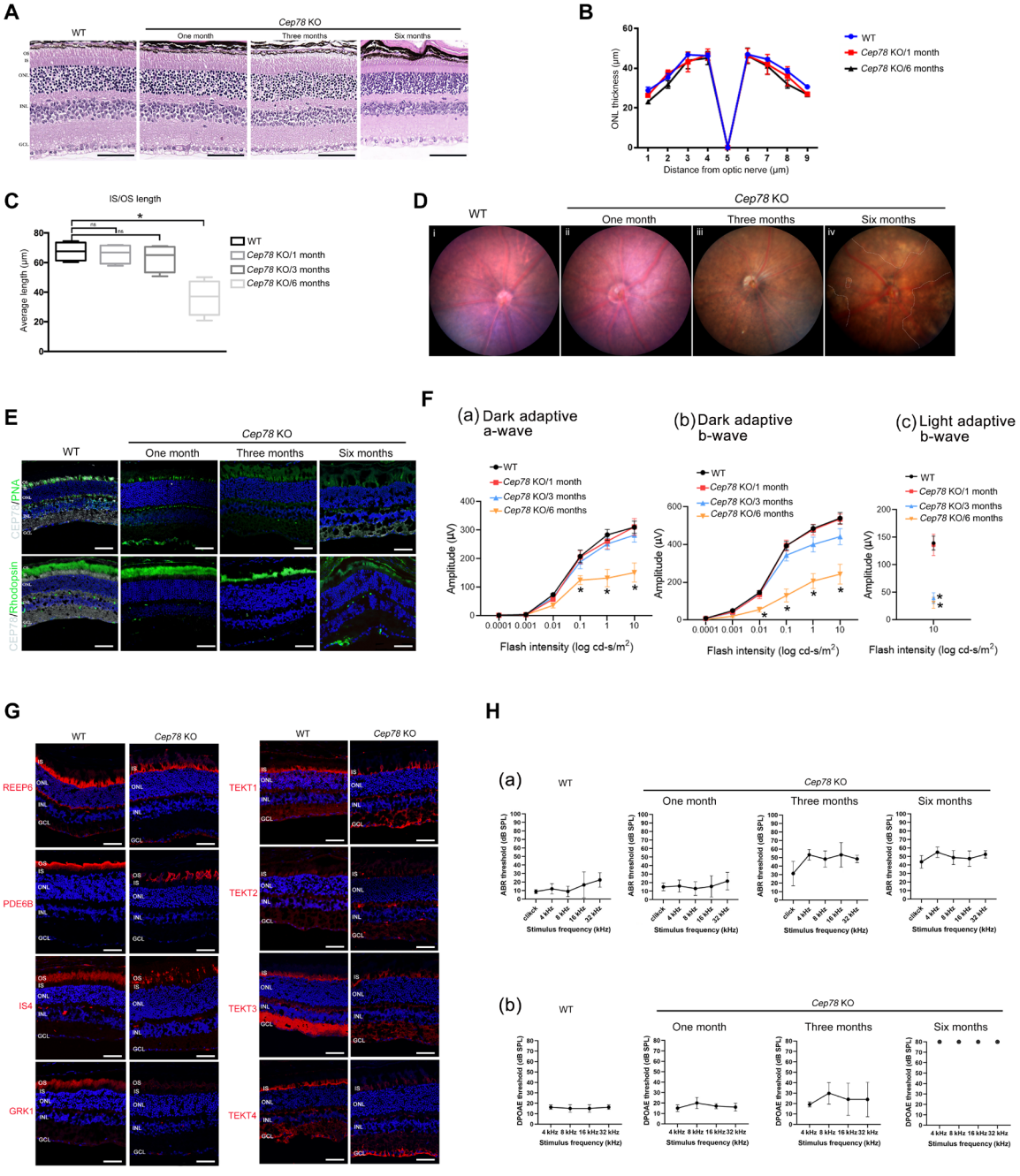

Fig. 7. The retina and hearing phenotypes of *Cep78* KO mice. (**A**) H&E staining of the retinal structure in WT and *Cep78* KO mice (scale bars, 100 μm). (**B**) Spider diagrams representing the thickness of the ONL of WT and *Cep78* KO mice at various distances from the optic nerve head (error bars, SEM). (**C**) Average length of IS/OS in mice with different ages (two-sided Student's *t* test; **P* < 0.05; error bars, SEM). (**D**) CFP of mice with different ages. (i) WT mice; (ii) 1-month-old *Cep78* KO mice; (iii) 3-month-old *Cep78* KO mice; (iv) 6-month-old *Cep78* KO mice. Dotted line marks atrophy areas. (**E**) Immunofluorescence staining for PNA, rhodopsin, and CEP78. CEP78 was undetectable in the IS of the retinas of *Cep78* KO mice compared to WT mice (scale bars, 100 μm). (**F**) Electroretinography recordings of *Cep78* KO mice with various ages. (a) a-wave in dark-adaptive responses; (b) b-wave in dark-adaptive responses; (c) b-wave in light-adaptive responses (two-sided Student's *t* test; **P* < 0.05; error bars, SEM). (**G**) Immunofluorescence staining for REEP6, PDE6b, IS4, GRK1, and Tektins in the retinas of WT and *Cep78* KO mice (scale bars, 100 μm). (**H**) ABR (a) and DPOAE (b) thresholds of *Cep78* KO mice at different ages (error bars, SEM). IPL, inner plexiform layer; OPL, outer plexiform layer; INL, inner nuclear layer; GCL, ganglion cell layer (*n* = 3 biologically independent WT mice and KO mice).

the third family, the proband (II:1) also displayed male infertility, while the fertility of his sibling carrying the same *CEP78* mutation was not documented. Therefore, further studies are needed to determine whether *CEP78* mutations are linked to male infertility. In our study, we revealed a large family with *CEP78* mutation and male sterility. Notably, the two infertile siblings exhibited diminished sperm counts and motility, aberrant sperm morphology, and impairments in sperm ultrastructure. Moreover, *Cep78* KO male mice exhibited the oligoasthenoteratospermia phenotype and infertility. Our findings thus confirm the crucial role for *CEP78* in

male infertility. Why did previous studies not suggest a relationship between *CEP78* variants and male infertility? We initially guessed that these mutations might be involved in generating different transcripts. However, when we analyzed the positions of the known mutations, we noticed that all of the reported mutations were located in each *CEP78* transcript. The possibility that these mutations may disturb various conserved domains of CEP78 was also excluded. Thus, we speculated that all of the patients were recruited by these studies because of the severe impairments in vision and hearing, and the element of male infertility might have been easily ignored. Last, in the reported 14 families with CRDHL syndrome, the pedigrees showed that only three families involving male patients had offspring, which may have been facilitated by assisted reproduction technologies. This finding may reasonably explain why patients had the same mutation, but one was infertile and another had offspring. Collectively, in the current study, we unraveled that loss-of-function mutations of *CEP78* can cause CRDHL syndrome accompanied by male infertility, which we have called CRDHLMI syndrome, and we also unveiled a causative gene for male infertility in humans and mice.

CEP78 localizes to the parental centrioles (*17*), which determine the position of the flagella and cilia and become the basal body of these organelles (*51*). Efforts to find the underlying mechanism of CEP78 in ciliogenesis are ongoing. CEP78 interacts with polo-like kinase 4 (Plk4) at centrioles and is required for Plk4-induced centriole overduplication (*17*). CEP78 binds specifically to EDD-DYRK2-DDB1^{VprBP} to impede the transfer of ubiquitin from phosphogluconate dehydratase (EDD) to CP110, which is pivotal for centriole length and cilia assembly (*47*). Recently, another study proposed that CEP78 interacts with CEP350 to promote ciliogenesis by negatively regulating CP110 levels via an EDD1-dependent mechanism (*52*). However, the CEP78 signaling pathway that is involved in spermatogenesis is completely unknown. In the current study, we performed a proteomics analysis on the testes of WT and *Cep78* KO male mice to understand the molecular mechanism of CEP78 in the spermatogenic process. Intriguingly, the sharply reduced expression of TEKT family members caught our attention, as the TEKT family plays a critical role in spermatogenesis (*40*–*46*). Mechanistically, we suggested that CEP78 regulated the expression of TEKT1, TEKT2, TEKT3, TEKT4, and TEKT5 by positively regulating the levels of USP16 via a ubiquitination-dependent pathway. In addition, CEP78 regulated H1-7 expression (the deficiency of which causes defects in sperm nuclear formation) by interacting with CETN1 to modulate sperm head development. Our findings elucidate the potential mechanisms by which CEP78 regulates sperm formation and provide additional insights for future research on the functions of CEP78 in spermatogenesis.

In reports of humans with *CEP78* mutations, the retinas showed cone-rod dystrophy caused by the degeneration of cone photoreceptors at a faster rate than rod photoreceptors. In *Cep78* KO mice, the functional change was first recorded in light-adapted rather than dark-adapted ERG responses, indicating that cones were also compromised earlier than rods in the mice. Although fundus imaging of patients carrying a *CEP78* mutation showed major vascular arcades surrounding the macula, the appearance of fundus images of *Cep78* KO mice was similar to that of retinitis pigmentosa. These differences might be because the mouse retinas are rod dominant. The characteristic of hearing loss caused by *CEP78* mutations is basically the same in both humans and *Cep78* KO mice, which is not congenital deafness but instead delayed hearing loss. Impairments in maintaining and supporting hair cell function but not damage in the developmental stage of hair cells mediated this type of hearing loss. However, in terms of degree, the hearing loss of the model mice was not as severe as that of humans. Most patients' high-frequency hearing loss was severe in their youth, while most of the high-frequency hearing loss of model mice was moderate. Therefore, research on hearing and vision in *Cep78* KO mice requires further exploration.

In conclusion, our work unveiled a unexplored role for CEP78 in human disease, reporting *CEP78* as a causative gene for male infertility. As an original finding, our research further elucidated the detailed molecular mechanism by which CEP78 regulates the spermatogenic process. Of particular concern is the poor prognosis of patients and mice with *CEP78* mutations after ICSI treatment, indicating that the identification of the causative genes associated with centrosome function may provide a clue for estimating the outcomes of ICSI treatment in infertile patients.

MATERIALS AND METHODS

Study participants

Two infertile siblings and their family members were recruited from West China Second University Hospital, Sichuan University, and 1000 healthy Chinese volunteers who had undergone a medical checkup without evidence of any infertility were enrolled as normal controls. In addition, 473 infertile individuals were recruited to determine the frequency of *CEP78* variants in a sporadic male sterile population. This study was conducted according to the tenets of the Declaration of Helsinki, and ethical approval was obtained from the Ethical Review Board of West China Second University Hospital, Sichuan University. All subjects signed an informed consent form.

WES and Sanger sequencing

Peripheral blood samples were obtained from all subjects, and the genomic DNA was extracted using a DNeasy blood and tissue kit (69504, Qiagen), according to the manufacturer's protocol. WES was performed on the proband using the SureSelectXT human all exon kit (5190-6209, Agilent Technologies) and HiSeq X-TEN system (Illumina). The reads were mapped to the human reference sequence (UCSC hg19) using BWA version 0.7.9a from the BWA-MEM algorithm. After quality filtration with the Genome Analysis Toolkit, functional annotation was performed using ANNOVAR through a series of databases, including the 1000Genomes Project, dbSNP, HGMD, and ExAC. Next, PolyPhen-2, SIFT, MutationTaster, and CADD were used for functional prediction. *CEP78* mutations identified using WES were confirmed using Sanger sequencing. The PCR primers are shown in table S2.

Mouse model

The animal experiments were approved by the Experimental Animal Management and Ethics Committee of West China Second University Hospital, Sichuan University. All animal procedures complied with the Animal Care and Use Committee of Sichuan University. We generated a *Cep78* KO mouse model using CRISPR-Cas9 technology. Exon 1 of the *Cep78*-201 (ENSMUST00000047704.8) transcript was recommended as the KO region. Briefly, Cas9 and single-guide RNAs were transcribed using T7 RNA polymerase in vitro and comicroinjected into the fertilized eggs of C57BL/6JGpt mice. The sequences of gRNA-1 and gRNA-2, as well as the protospacer adjacent motif

(PAM) site, are listed in table S2. Fertilized eggs were transplanted to obtain positive F0 mice, which were confirmed using PCR and sequencing. A stable F1 generation was obtained by mating positive F0 generation mice with C57BL/6JGpt mice. The genotype of *Cep78* KO mice was validated by performing PCR with specific primers (table S2). Here, 501 bp (primer F2/R2) of the band represented WT mice, 387 bp (primer F1/R1) of the band represented KO mice, and both bands were detected in heterozygote mice.

Mini-gene assay

A mini-gene assay was used to assess the effect of the splice site mutation (c.1069+1G>A). Exon 8, intron 9, and exon 9 of WT *CEP78* and mutant *CEP78* were amplified using specific primer 1 (table S2). The amplified fragments were cloned into a pSPL3 vector at the Eco RI and Bam HI sites using the ClonExpress II one-step cloning kit (C112-02, Vazyme). Human embryonic kidney (HEK) 293T cells were transfected with 1 μg of plasmid DNA containing WT or mutant alleles using low-toxicity Lipofectamine 3000 Reagent (L3000008, Thermo Fisher Scientific). Then, total cellular RNA was extracted from cells using GeneJET RNA (K0731, Thermo Fisher Scientific), and cDNAs were generated from total RNA using ReverTra Ace qPCR RT master mix (FSQ-201, Toyobo). The cDNA templates were amplified with TaKaRa Ex Taq (HRR001A, Takara) and primers located in the two cassette exons of the pSPL3 vector. The two primers were also as shown in table S2. Gel electrophoresis and Sanger sequencing were adopted to analyze PCR products and revealed an abnormally large transcript produced by *CEP78* splicing mutation.

Proteomic analysis

Testicular tissue samples from 8-week-old mice were used for a liquid chromatography–tandem mass spectrometry analysis with a standard protocol. The basic flow was described below. (i) The tissue was ground in liquid nitrogen, lysis buffer (8 M of urea, 1% protease inhibitor cocktail) was added, sonication with a high-intensity ultrasonic processor (Scientz) was performed, and the protein concentration in the supernatant was determined using a protein concentration assay (ab102536, Abcam); (ii) the protein supernatant was digested to produce peptides, purified reconstituted in 0.5 M triethylammonium bicarbonate (TEAB), and processed with a TMT kit (90111, Thermo Fisher Scientific) according to the manufacturer's instruction; (iii) liquid chromatography–tandem mass spectrometry was performed to identify and quantify the peptides using a Q Exactive HF-X mass spectrometer (Thermo Fisher Scientific) equipped with a Finnigan Nanospray II electrospray ionization source; (iv) raw data were analyzed using GO annotation (http://ebi.ac.uk/GOA/), domain annotation (InterProScan), and Kyoto Encyclopedia of Genes and Genomes pathway annotation (Kyoto Encyclopedia of Genes and Genomes online service tool KAAS mapper) software. Computational predictions in STRING (https://string-db.org/) were used to conduct protein-protein interaction network analyses.

Western blotting and Co-IP

Proteins were extracted from cells and mouse testes tissues using radioimmunoprecipitation buffer (P0013B, Beyotime) supplemented with protease inhibitor cocktail (P5726, Sigma-Aldrich), SDS sample loading buffer (P0015, Beyotime) was added, and samples were boiled at 95°C for 10 min. The denatured proteins were separated by SDS–polyacrylamide gel electrophoresis and transferred to polyvinylidene difluoride membranes (IPFL00010, Millipore). After incubation with tris-buffered saline–Tween 20 (TBST) containing 5% milk for 1 hour, the membrane was incubated with primary and secondary antibodies diluted in TBST containing 5% milk. Chemiluminescence with enhanced chemiluminescence chemical substrate (WBKLS0100, Millipore) was applied for immunoblot analyses.

For Co-IP assays, extracted proteins were incubated with primary antibody–coupled Protein A/G beads (USA88803, Invitrogen) overnight at 4°C. The beads were washed with washing buffer [50 mM tris-HCl (pH 7.4), 0.1% Triton X-100, and 500 mM NaCl], eluted with 2× SDS loading buffer, and boiled for 15 min at 75°C. Last, the products were separated using SDS–polyacrylamide gel electrophoresis and analyzed using immunoblotting procedures. Detailed information on the primary antibodies and secondary antibodies used for Western blotting and Co-IP is listed in table S3.

Immunofluorescence staining and histological assay

For germ cell immunostaining, samples were fixed with 4% paraformaldehyde, permeabilized with 0.1% Triton X-100 (HFH10, Invitrogen) for 10 min, and blocked with 3% bovine serum albumin (A1933, Sigma-Aldrich) for 1 hour at 25°C. Next, the samples were incubated with primary antibodies overnight at 4°C, followed by 1 hour of incubation with secondary antibodies at room temperature. Nuclei were counterstained with 4′,6-diamidino-2-phenylindole (DAPI) (D9542, Sigma-Aldrich).

For the staining of testicular tissues, samples were first fixed with 3.7% formaldehyde in phosphate-buffered saline (PBS). After subsequent dehydration with an ethanol gradient, tissues were embedded in paraffin and sectioned into 5-μm slices. After deparaffination and rehydration, sections were processed with 3% hydrogen peroxide for 10 min at room temperature, and antigen retrieval was performed by incubating sections with 20 mM sodium citrate for 15 min at 95°C. After cooling overnight, the samples were incubated with primary antibodies at 4°C overnight and underwent a 1-hour incubation with secondary antibodies at room temperature. Nuclei were stained with DAPI (D9542, Sigma-Aldrich). Eyeballs were fixed with 4% paraformaldehyde in 0.1 M PBS (pH 7.4) at 4°C for 1 hour, dehydrated in 30% sucrose overnight, and embedded in optimal cutting temperature compound. Sections were cut at 8 mm with a cryostat, collected on glass slides, and stored at −20°C. The retinal sections were then incubated with blocking solution (5% normal donkey serum) for 1 hour and incubated with primary antibodies overnight at 4°C. Subsequently, sections were incubated with a secondary antibody for 1 hour at room temperature in the dark. Last, sections were counterstained with DAPI (D9542, Sigma-Aldrich) and mounted with Mowiol mounting medium. Images were captured with a confocal microscope (FV3000, Olympus Corporation). Detailed information on the antibodies is provided in table S3. For the histological assay, paraffin sections of the samples were stained with H&E and observed under a microscope (Axio Imager 2, Zeiss).

Acridine orange staining

The acridine orange staining of mouse embryos was performed according to the previous study with slight modifications (*53*). Briefly, the embryo samples were first fixed with cold 4% paraformaldehyde for 30 min. After washing with 1× PBS buffer twice, the samples were incubated with 0.3% Triton X-100 for 20 min at 4°C. Next, the embryos were incubated with acridine orange (10 μg/ml; 494-38-2, Sigma-Aldrich) diluted with 1× PBS for 15 min at room temperature. The stained embryos were ready to observe after being washed

with 1× PBS three times. The acridine orange staining of sperm followed the methods described in a previous study (*54*). The sperm cells from mice were fixed onto slides with TNE buffer [50 mM tris-HCl (pH 7.4), 100 mM NaCl, 0.1 mM EDTA] for 30 min and then perforated with 0.5% Triton X-100 for 20 min. Subsequently, the slides were incubated with acridine orange solution [acridine orange (50 μg /ml) in buffer: 0.1 M citric acid, 0.2 M Na_2HPO_4, 0.15 M NaCl, and 1 mM EDTA (pH 6)] for 3 min at room temperature. Then, the slides were washed with 1× PBS twice. All samples were observed under a laser scanning confocal microscope (Olympus FV3000, Japan). Acridine orange fluorescence was excited at 488 nm, and images were collected at 600 to 650 nm (red) or 500 to 550 nm (green), respectively.

Electron microscopy

For SEM, the sperm cells were fixed onto slides using 2.5% glutaraldehyde and refrigerated overnight at 4°C. After rinsing the cells with 1× PBS buffer three times, cells were gradually dehydrated with an ethanol gradient (30, 50, 75, 95, and 100% ethanol) and dried using a CO_2 critical-point dryer. After metal spraying with an ionic sprayer meter (Eiko E-1020, Hitachi), the samples were observed by SEM (S-3400, Hitachi).

For TEM, samples were fixed routinely with 3% glutaraldehyde and osmium tetroxide. Thereafter, samples were subjected to post-fixation with 1% OSO_4 and sucrose and dehydrated with graded concentrations of ethanol. Next, the samples were embedded in Epon 812. Ultrathin sections were stained with uranyl acetate and lead citrate and then observed using a TEM (TECNAI G2 F20, Philips) with an accelerating voltage of 80 kV.

RNA isolation and RT-PCR

Total RNA was extracted from samples using GeneJET RNA (K0731, Thermo Fisher Scientific) and transcribed into cDNA using ReverTra Ace qPCR RT master mix (FSQ-201, Toyobo) according to the manufacturer's instructions. All RT-PCR primers are follows in table S2.

STA-PUT velocity sedimentation

Spermatogenic cells were obtained through cell density gradient centrifugation using the STA-PUT velocity sedimentation method described previously (*55*, *56*). Briefly, mouse germ cells were first collected from seminiferous tubules; then, total spermatogenic cells were diluted in a 0.5% bovine serum albumin solution, and cell aggregates were filtered using an 80-mm mesh. Subsequently, gradient separation of germ cells was performed using an STA-PUT velocity sedimentation cell separator (ProScience). Germ cells at different stages were extracted for subsequent analysis.

Cell culture, transfection, and treatments

HEK293T cells (CRL-11268) and hRPE1 cells (CRL-4000) were purchased from the American Type Culture Collection. Dulbecco's modified Eagle's medium (11-995-065, Gibco) with 10% fetal bovine serum (10-082-147, Gibco) was used to culture HEK293T cells, and Dulbecco's modified Eagle's medium/F12 (A4192001, Gibco) supplemented with 10% fetal bovine serum (10-082-147, Gibco) was used to culture hRPE1 cells. The expression plasmids pcDNA3.1-Myc-WT-*CEP78*, pcDNA3.1-Myc-Mutant-*CEP78*, and pEGFP-N1-*USP16* and lentivirus vectors pLKO.1-EGFP-sh*CEP78* and pLKO.1-EGFP-sh*USP16* were constructed by Vigene Biosciences (Jinan, China). The target sequences of shRNA were listed in table S2. The plasmids were transfected into cells with Lipofectamine 3000 (L3000008, Thermo Fisher Scientific), and lentivirus transfection was performed using reagents provided by the manufacturer. For PR-619 (S7130, Selleck Chemicals) treatment, various concentrations (10, 15, and 20 μM) of PR-619 diluted in dimethyl sulfoxide were added to hRPE1 cells and incubated for 8 hours. For MG132 (M8699, Sigma-Aldrich) treatment, hRPE1 cells were infected with pLKO.1-EGFP-sh*USP16* or the control vector for 72 hours and subsequently treated with 10 μM MG132 for 6 hours. Last, the cells were harvested to extract proteins for immunoblotting assays.

Intracytoplasmic sperm injection

ICSI was performed using standard techniques as previously described (*57*). Briefly, female KM mice were first injected with 5 IU of equine chorionic gonadotropin (CG) (HOR-272, ProSpec). After 48 hours, the female mice were injected with 5 IU of human CG (M2530, Easycheck) again to acquire MII-arrested oocytes. MII-arrested oocytes were incubated with Chatot-Ziomek-Bavister medium (M2750, Easycheck) at 37.5°C in an incubator with 5% CO_2. Mouse spermatozoa from cauda epididymides were incubated in HTF (human tubal fluid) medium (M1150, Easycheck). After freezing and thawing, a single sperm head was obtained and microinjected into an MII oocyte using a NIKON inverted microscope and a Piezo device (PrimeTech) in Whitten's-Hepes medium containing 0.01% polyvinyl alcohol (12360-038, Gibco) and cytochalasin B (3.5 μg/ml; C-6762, Sigma-Aldrich). Once the injection was completed successfully, the oocytes were transferred into G1-Plus medium (10132, Vitrolife) at 37.5°C in an incubator with 5% CO_2 in air.

ERG analysis

Both dark-adapted and light-adapted ERG images (Diagnosys LLC, Lowell, MA, USA) were recorded from mice at the ages of 1, 3, and 6 months. For dark-adapted responses, the mice were dark-adapted overnight and anesthetized with a mixture of ketamine and xylazine (90 mg/kg ketamine combined with 8 mg/kg xylazine), and pupils were dilated with 0.5% tropicamide and 0.5% phenylephrine hydrochloride. Full-field ERG images were recorded after subcutaneously inserting a ground electrode near the tail and a reference electrode in the back. A golden-ring electrode was gently positioned on the cornea. All procedures were performed under dim red light. The amplitude of the a-wave was measured from the baseline to the peak of the a-wave, and the b-wave was measured from the nadir of the a-wave to the apex of the b-wave peak.

CFP test

For CFP, the mice were anesthetized with a mixture of ketamine and xylazine (90 mg/kg ketamine combined with 8 mg/kg xylazine), and their pupils were dilated with 0.5% tropicamide and 0.5% phenylephrine hydrochloride. The CFPs were captured with the MICRON IV system (Phoenix Technology Group, Pleasanton, CA, USA).

Auditory brainstem response

The mice were anesthetized with a mixture of esketamine and xylazine (50 mg/kg esketamine combined with 25 mg/kg xylazine) and placed in a soundproof chamber. The recording electrode was placed halfway between the pinnae on the vertex of the cranium, the reference electrode was placed on the left mastoid surface, and the ground electrode was positioned at the buttock. All ABR tests were

conducted in a free field, and sound stimuli were delivered by a loudspeaker (SN 2422, multifunction speaker, Tucker-Davis Technologies) placed at a distance of 10 cm from the mouse ear. Experiments were performed using the TDT BioSigRZ platform (version 5.7.5) driven by the RZ6 multi-I/O processor (Tucker-Davis Technologies). The clicks were presented at a rate of 21.2/s with a 10-ms scanning time and 1024 repetitions. Tone bursts with frequencies of 4 to 32 kHz were presented for a 5-ms duration with a 1-ms on/off ramp time and presented at a rate of 10/s with 400 repetitions. Stimuli were presented from 90 to 20 dB SPL in 5 dB steps. ABR thresholds were defined as the lowest stimulus level where recognizable features of the waveform were repeatable. Only the left ears were tested for the presence of tags on the right ears.

Distortion product otoacoustic emissions

DPOAEs were evoked by two primary stimulus tones, f1 and f2 (f2/f1 = 1.22), and recorded at 2f1 – f2 in response to the stimulus. The primary level of the stimulus was 70 dB, decreasing in 10-dB intervals with 256 repetitions. The DPOAEs were recorded using a low-noise microphone (SN 2421, 2422, multifunction speaker, Tucker-Davis Technologies). Experiments were performed using the BioSigRZ software driven by the RZ6 multi-I/O processor (Tucker-Davis Technologies). The cutoff value for an evoked DPOAE was 3 dB above the SD of the noise.

Statistical analysis

The GraphPad Prism version 8.4.0 software program and Statistical Package for the Social Sciences version 17.0 software program were used for statistical analyses (IBM Corporation, Armonk, NY, USA). All data are presented as the mean ± SEM values. *P* values of less than 0.05 were considered statistically significant. The two-sided Student's *t* test was used to compare the observed indices between the experimental groups.

SUPPLEMENTARY MATERIALS

Supplementary material for this article is available at https://science.org/doi/10.1126/sciadv.abn0968

View/request a protocol for this paper from *Bio-protocol*.

REFERENCES AND NOTES

1. C. L. R. Barratt, L. Bjorndahl, C. J. De Jonge, D. J. Lamb, F. Osorio Martini, R. McLachlan, R. D. Oates, S. van der Poel, B. S. John, M. Sigman, R. Sokol, H. Tournaye, The diagnosis of male infertility: An analysis of the evidence to support the development of global WHO guidance-challenges and future research opportunities. *Hum. Reprod. Update* **23**, 660–680 (2017).
2. H. Tournaye, C. Krausz, R. D. Oates, Novel concepts in the aetiology of male reproductive impairment. *Lancet Diabetes Endocrinol.* **5**, 544–553 (2017).
3. S. Y. Jiao, Y. H. Yang, S. R. Chen, Molecular genetics of infertility: Loss-of-function mutations in humans and corresponding knockout/mutated mice. *Hum. Reprod. Update* **27**, 154–189 (2021).
4. M. Bornens, The centrosome in cells and organisms. *Science* **335**, 422–426 (2012).
5. T. Avidor-Reiss, Rapid evolution of sperm produces diverse centriole structures that reveal the most rudimentary structure needed for function. *Cell* **7**, 67 (2018).
6. Y. Sha, X. Wang, J. Yuan, X. Zhu, Z. Su, X. Zhang, X. Xu, X. Wei, Loss-of-function mutations in centrosomal protein 112 is associated with human acephalic spermatozoa phenotype. *Clin. Genet.* **97**, 321–328 (2020).
7. Y. W. Sha, X. Xu, L. B. Mei, P. Li, Z. Y. Su, X. Q. He, L. Li, A homozygous CEP135 mutation is associated with multiple morphological abnormalities of the sperm flagella (MMAF). *Gene* **633**, 48–53 (2017).
8. D. Sinha, M. Kalimutho, J. Bowles, A. L. Chan, D. J. Merriner, A. L. Bain, J. L. Simmons, R. Freire, J. A. Lopez, R. M. Hobbs, M. K. O'Bryan, K. K. Khanna, Cep55 overexpression causes male-specific sterility in mice by suppressing Foxo1 nuclear retention through sustained activation of PI3K/Akt signaling. *FASEB J.* **32**, 4984–4999 (2018).
9. S. Yuan, C. J. Stratton, J. Bao, H. Zheng, B. P. Bhetwal, R. Yanagimachi, W. Yan, Spata6 is required for normal assembly of the sperm connecting piece and tight head-tail conjunction. *Proc. Natl. Acad. Sci. U.S.A.* **112**, E430–E439 (2015).
10. E. A. Hall, M. Keighren, M. J. Ford, T. Davey, A. P. Jarman, L. B. Smith, I. J. Jackson, P. Mill, Acute versus chronic loss of mammalian Azi1/Cep131 results in distinct ciliary phenotypes. *PLOS Genet.* **9**, e1003928 (2013).
11. S. S. Siller, H. Sharma, S. Li, J. Yang, Y. Zhang, M. J. Holtzman, W. Winuthayanon, H. Colognato, B. C. Holdener, F. Q. Li, K. I. Takemaru, Conditional knockout mice for the distal appendage protein CEP164 reveal its essential roles in airway multiciliated cell differentiation. *PLOS Genet.* **13**, e1007128 (2017).
12. J. Kim, J. T. Kwon, J. Jeong, J. Kim, S. H. Hong, J. Kim, Z. Y. Park, K. H. Chung, E. M. Eddy, C. Cho, SPATC1L maintains the integrity of the sperm head-tail junction. *EMBO Rep.* **19**, e45991 (2018).
13. P. Avasthi, J. F. Scheel, G. Ying, J. M. Frederick, W. Baehr, U. Wolfrum, Germline deletion of Cetn1 causes infertility in male mice. *J. Cell Sci.* **126**, 3204–3213 (2013).
14. G. Luo, M. Hou, B. Wang, Z. Liu, W. Liu, T. Han, D. Zhang, X. Zhou, W. Jia, Y. Tan, Y. Wu, J. Wang, X. Zhang, Tsga10 is essential for arrangement of mitochondrial sheath and male fertility in mice. *Andrology* **9**, 368–375 (2021).
15. Y. Ye, X. Wei, Y. Sha, N. Li, X. Yan, L. Cheng, D. Qiao, W. Zhou, R. Wu, Q. Liu, Y. Li, Loss-of-function mutation in TSGA10 causes acephalic spermatozoa phenotype in human. *Mol. Genet. Genomic Med.* **8**, e1284 (2020).
16. X. Zhang, L. Wang, Y. Ma, Y. Wang, H. Liu, M. Liu, L. Qin, J. Li, C. Jiang, X. Zhang, X. Shan, Y. Liu, J. Li, Y. Li, R. Zheng, Y. Sun, J. Sun, X. Leng, Y. Liang, F. Zhang, X. Jiang, Y. Yang, Y. Shen, CEP128 is involved in spermatogenesis in humans and mice. *Nat. Commun.* **13**, 1395 (2022).
17. K. Brunk, M. Zhu, F. Barenz, A. S. Kratz, U. Haselmann-Weiss, C. Antony, I. Hoffmann, Cep78 is a new centriolar protein involved in Plk4-induced centriole overduplication. *J. Cell Sci.* **129**, 2713–2718 (2016).
18. J. Azimzadeh, M. L. Wong, D. M. Downhour, A. Sánchez Alvarado, W. F. Marshall, Centrosome loss in the evolution of planarians. *Science* **335**, 461–463 (2012).
19. P. Namburi, R. Ratnapriya, S. Khateb, C. H. Lazar, Y. Kinarty, A. Obolensky, I. Erdinest, D. Marks-Ohana, E. Pras, T. Ben-Yosef, H. Newman, M. Gross, A. Swaroop, E. Banin, D. Sharon, Bi-allelic truncating mutations in CEP78, encoding centrosomal protein 78, cause cone-rod degeneration with sensorineural hearing loss. *Am. J. Hum. Genet.* **99**, 777–784 (2016).
20. K. Nikopoulos, P. Farinelli, B. Giangreco, C. Tsika, B. Royer-Bertrand, M. K. Mbefo, N. Bedoni, U. Kjellstrom, I. El Zaoui, S. A. Di Gioia, S. Balzano, K. Cisarova, A. Messina, S. Decembrini, S. Plainis, S. V. Blazaki, M. I. Khan, S. Micheal, K. Boldt, M. Ueffing, A. P. Moulin, F. P. M. Cremers, R. Roepman, Y. Arsenijevic, M. K. Tsilimbaris, S. Andréasson, C. Rivolta, Mutations in CEP78 cause cone-rod dystrophy and hearing loss associated with primary-cilia defects. *Am. J. Hum. Genet.* **99**, 770–776 (2016).
21. G. Ascari, F. Peelman, P. Farinelli, T. Rosseel, N. Lambrechts, K. A. Wunderlich, M. Wagner, K. Nikopoulos, P. Martens, I. Balikova, L. Derycke, G. Holtappels, O. Krysko, T. Van Laethem, S. De Jaegere, B. Guillemyn, R. De Rycke, J. De Bleecker, D. Creytens, J. Van Dorpe, J. Gerris, C. Bachert, C. Neuhofer, S. Walraedt, A. Bischoff, L. B. Pedersen, T. Klopstock, C. Rivolta, B. P. Leroy, E. De Baere, F. Coppieters, Functional characterization of the first missense variant in CEP78, a founder allele associated with cone-rod dystrophy, hearing loss, and reduced male fertility. *Hum. Mutat.* **41**, 998–1011 (2020).
22. G. Ascari, N. D. Rendtorff, M. De Bruyne, J. De Zaeytijd, M. Van Lint, M. Bauwens, M. Van Heetvelde, G. Arno, J. Jacob, D. Creytens, J. Van Dorpe, T. Van Laethem, T. Rosseel, T. De Pooter, P. De Rijk, W. De Coster, B. Menten, A. D. Rey, M. Strazisar, M. Bertelsen, L. Tranebjaerg, E. De Baere, Long-read sequencing to unravel complex structural variants of *CEP78* leading to cone-rod dystrophy and hearing loss. *Front. Cell Dev. Biol.* **9**, 664317 (2021).
23. F. O. Desmet, D. Hamroun, M. Lalande, G. Collod-Beroud, M. Claustres, C. Beroud, Human splicing finder: An online bioinformatics tool to predict splicing signals. *Nucleic Acids Res.* **37**, e67 (2009).
24. J. M. Schwarz, C. Rodelsperger, M. Schuelke, D. Seelow, MutationTaster evaluates disease-causing potential of sequence alterations. *Nat. Methods* **7**, 575–576 (2010).
25. T. Avidor-Reiss, E. L. Fishman, It takes two (centrioles) to tango. *Reproduction* **157**, R33–R51 (2019).
26. T. Avidor-Reiss, M. Mazur, E. L. Fishman, P. Sindhwani, The role of sperm centrioles in human reproduction—The known and the unknown. *Front. Cell Dev. Biol.* **7**, 188 (2019).
27. M. Cissen, M. V. Wely, I. Scholten, S. Mansell, J. P. Bruin, B. W. Mol, D. Braat, S. Repping, G. Hamer, Measuring sperm DNA fragmentation and clinical outcomes of medically assisted reproduction: A systematic review and meta-analysis. *PLOS ONE* **11**, e0165125 (2016).
28. H. Norppa, G. C. Falck, What do human micronuclei contain? *Mutagenesis* **18**, 221–233 (2003).
29. T. Pauerova, L. Radonova, K. Kovacovicova, L. Novakova, M. Skultety, M. Anger, Aneuploidy during the onset of mouse embryo development. *Reproduction* **160**, 773–782 (2020).

30. T. Igakura, K. Kadomatsu, T. Kaname, H. Muramatsu, Q. W. Fan, T. Miyauchi, Y. Toyama, N. Kuno, S. Yuasa, M. Takahashi, T. Senda, O. Taguchi, K. Yamamura, K. Arimura, T. Muramatsu, A null mutation in basigin, an immunoglobulin superfamily member, indicates its important roles in peri-implantation development and spermatogenesis. *Dev. Biol.* **194**, 152–165 (1998).
31. M. Siva, S. Haberecht-Müller, M. Prochazkova, J. Prochazka, F. Sedlak, K. Chawengsaksophak, P. Kasparek, R. Sedlacek, J. Konvalinka, E. Krüger, K. G. Saskova, DDI2 protease activity controls embryonic development and inflammation via TCF11/NRF1. bioRxiv 2020.12.16.423023 [**Preprint**]. 16 December 2020. https://doi.org/10.1101/2020.12.16.423023.
32. Y. Hou, Z. Wu, Y. Zhang, H. Chen, J. Hu, Y. Guo, Y. Peng, Q. Wei, Functional analysis of hydrolethalus syndrome protein HYLS1 in ciliogenesis and spermatogenesis in Drosophila. *Front. Cell Dev. Biol.* **8**, 301 (2020).
33. S. Sonn, Y. Jeong, K. Rhee, Nip2/centrobin may be a substrate of Nek2 that is required for proper spindle assembly during mitosis in early mouse embryos. *Mol. Reprod. Dev.* **76**, 587–592 (2009).
34. K. Lin, S. Zhang, Q. Shi, M. Zhu, L. Gao, W. Xia, B. Geng, Z. Zheng, E. Y. Xu, Essential requirement of mammalian Pumilio family in embryonic development. *Mol. Biol. Cell* **29**, 2922–2932 (2018).
35. S. G. Morham, K. D. Kluckman, N. Voulomanos, O. Smithies, Targeted disruption of the mouse topoisomerase I gene by camptothecin selection. *Mol. Cell. Biol.* **16**, 6804–6809 (1996).
36. D. Wang, W. Wang, P. Dawkins, T. Paterson, N. Kalsheker, J. M. Sallenave, A. M. Houghton, Deletion of Serpina1a, a murine α1-antitrypsin ortholog, results in embryonic lethality. *Exp. Lung Res.* **37**, 291–300 (2011).
37. M. P. Baggelaar, H. den Dulk, B. I. Florea, D. Fazio, N. Bernabo, M. Raspa, A. P. A. Janssen, F. Scavizzi, B. Barboni, H. S. Overkleeft, M. Maccarrone, M. van der Stelt, ABHD2 inhibitor identified by activity-based protein profiling reduces acrosome reaction. *ACS Chem. Biol.* **14**, 2295–2304 (2019).
38. Z. Zhang, G. L. Wang, H. X. Li, L. Li, Q. W. Cui, C. B. Wei, F. Zhou, Regulation of fertilization in male rats by CatSper2 knockdown. *Asian J. Androl.* **14**, 301–309 (2012).
39. M. S. Girault, S. Dupuis, C. Ialy-Radio, L. Stouvenel, C. Viollet, R. Pierre, M. Favier, A. Ziyyat, S. Barbaux, Deletion of the Spata3 gene induces sperm alterations and in vitro hypofertility in mice. *Int. J. Mol. Sci.* **22**, 1959 (2021).
40. H. Tanaka, N. Iguchi, Y. Toyama, K. Kitamura, T. Takahashi, K. Kaseda, M. Maekawa, Y. Nishimune, Mice deficient in the axonemal protein Tektin-t exhibit male infertility and immotile-cilium syndrome due to impaired inner arm dynein function. *Mol. Cell. Biol.* **24**, 7958–7964 (2004).
41. A. Roy, Y. N. Lin, J. E. Agno, F. J. DeMayo, M. M. Matzuk, Tektin 3 is required for progressive sperm motility in mice. *Mol. Reprod. Dev.* **76**, 453–459 (2009).
42. W. Cao, T. W. Ijiri, A. P. Huang, G. L. Gerton, Characterization of a novel tektin member, TEKT5, in mouse sperm. *J. Androl.* **32**, 55–69 (2011).
43. M. Larsson, J. Norrander, S. Graslund, E. Brundell, R. Linck, S. Stahl, C. Hoog, The spatial and temporal expression of Tekt1, a mouse tektin C homologue, during spermatogenesis suggest that it is involved in the development of the sperm tail basal body and axoneme. *Eur. J. Cell Biol.* **79**, 718–725 (2000).
44. S. Oiki, E. Hiyama, T. Gotoh, H. Iida, Localization of Tektin 1 at both acrosome and flagella of mouse and bull spermatozoa. *Zoolog. Sci.* **31**, 101–107 (2014).
45. A. Roy, Y. N. Lin, J. E. Agno, F. J. DeMayo, M. M. Matzuk, Absence of tektin 4 causes asthenozoospermia and subfertility in male mice. *FASEB J.* **21**, 1013–1025 (2007).
46. L. A. Amos, The tektin family of microtubule-stabilizing proteins. *Genome Biol.* **9**, 229 (2008).
47. D. Hossain, Y. Javadi Esfehani, A. Das, W. Y. Tsang, Cep78 controls centrosome homeostasis by inhibiting EDD-DYRK2-DDB1^{VprBP}. *EMBO Rep.* **18**, 632–644 (2017).
48. S. Urbe, H. Liu, S. D. Hayes, C. Heride, D. J. Rigden, M. J. Clague, Systematic survey of deubiquitinase localization identifies USP21 as a regulator of centrosome- and microtubule-associated functions. *Mol. Biol. Cell* **23**, 1095–1103 (2012).
49. H. Tanaka, N. Iguchi, A. Isotani, K. Kitamura, Y. Toyama, Y. Matsuoka, M. Onishi, K. Masai, M. Maekawa, K. Toshimori, M. Okabe, Y. Nishimune, HANP1/H1T2, a novel histone H1-like protein involved in nuclear formation and sperm fertility. *Mol. Cell. Biol.* **25**, 7107–7119 (2005).
50. Q. Fu, M. Xu, X. Chen, X. Sheng, Z. Yuan, Y. Liu, H. Li, Z. Sun, H. Li, L. Yang, K. Wang, F. Zhang, Y. Li, C. Zhao, R. Sui, R. Chen, *CEP78* is mutated in a distinct type of Usher syndrome. *J. Med. Genet.* **54**, 190–195 (2017).
51. E. A. Nigg, J. W. Raff, Centrioles, centrosomes, and cilia in health and disease. *Cell* **139**, 663–678 (2009).
52. A. B. Goncalves, S. K. Hasselbalch, B. B. Joensen, S. Patzke, P. Martens, S. K. Ohlsen, M. Quinodoz, K. Nikopoulos, R. Suleiman, M. P. Damso Jeppesen, C. Weiss, S. T. Christensen, C. Rivolta, J. S. Andersen, P. Farinelli, L. B. Pedersen, CEP78 functions downstream of CEP350 to control biogenesis of primary cilia by negatively regulating CP110 levels. *eLife* **10**, e63731 (2021).
53. M. Hayashi, T. Sofuni, M. Ishidate Jr., An application of acridine orange fluorescent staining to the micronucleus test. *Mutat. Res.* **120**, 241–247 (1983).
54. O. Ammar, M. Mehdi, M. Muratori, Teratozoospermia: Its association with sperm DNA defects, apoptotic alterations, and oxidative stress. *Andrology* **8**, 1095–1106 (2020).
55. V. R. Fantin, Q. Wang, G. E. Lienhard, S. R. Keller, Mice lacking insulin receptor substrate 4 exhibit mild defects in growth, reproduction, and glucose homeostasis. *Am. J. Physiol. Endocrinol. Metab.* **278**, E127–E133 (2000).
56. F. Alipour, M. Jalali, M. R. Nikravesh, A. Fazel, M. Sankian, E. Khordad, Assessment of sperm morphology, chromatin integrity, and catSper genes expression in hypothyroid mice. *Acta Biol. Hung.* **69**, 244–258 (2018).
57. R. Yanagimachi, Intracytoplasmic sperm injection experiments using the mouse as a model. *Hum. Reprod.* **13** (Suppl. 1), 87–98 (1998).

Acknowledgments: We thank the patients and their family members for their support during this research study. We thank laboratory animal center of Huazhong Agricultural University for ICSI assay. **Funding:** This study was funded by the National Key Research and Development Project (2019YFA0802101). This work was also supported by the West China Second University Hospital of Sichuan University (KS369). **Author contributions:** Y.S. designed and supervised the study experiments. Yihong Yang and Y.W. collected data and conducted the clinical evaluations. Xueguang Zhang, R.Z., and Y.S. performed experiments and analyzed most of the data. Xiaozhen Zhang and S.C. generated the CRISPR mice. C.L., Yang Yang, and Q.R. analyzed the retinal function of mice. H.L. analyzed the hearing of mice. Y.M., Mohan Liu, Man Liu, and C.J. performed experiments. Y.S. wrote the manuscript, with input from the other authors. W.Z. and S.C. provided valuable advice for the manuscript. All authors revised and approved the article. **Competing interests:** The authors declare that they have no competing interests. **Data and materials availability:** All data needed to evaluate the conclusions in the paper are present in the paper and/or the Supplementary Materials.

Submitted 7 December 2021
Accepted 22 August 2022
Published 7 October 2022
10.1126/sciadv.abn0968